Encoding arbitrary four-qubit states in the spatial parity of a photon pair

Ayman F. Abouraddy,[1,*] Timothy M. Yarnall,[2,†] Giovanni Di Giuseppe,[1,3] Malvin C. Teich,[1,4] and Bahaa E. A. Saleh[1]
[1]*CREOL, The College of Optics & Photonics, University of Central Florida, Orlando, Florida 32816, USA*
[2]*19 Chestnut Circle, Merrimack, New Hampshire 03054, USA*
[3]*School of Science and Technology, Physics Division, University of Camerino, 62032 Camerino, Italy*
[4]*Departments of Electrical & Computer Engineering and Physics, Boston University, Boston, Massachusetts 02215, USA*
(Received 8 March 2012; published 21 June 2012)

Advancing quantum information processing is predicated on the preparation of ever-larger multiqubit states. Photonic realizations of such states may be achieved by increasing the number of photons populating the state or the number of qubits encoded per photon. Typical approaches to the latter strategy utilize distinct degrees of freedom of the photon field. We present here an approach that encodes two qubits per photon in the *spatial parity* of its transverse spatial profile. Simple linear optical devices transform each parity qubit separately or the two qubits jointly. Furthermore, we demonstrate that entangled photon pairs produced by spontaneous parametric down-conversion may be used to prepare *arbitrary four-qubit states* through sculpting the spatial profile of the classical optical pump. Two examples are highlighted—the preparation of two-photon four-qubit Greenberger-Horne-Zeilinger and *W* states, whose encoding in a photon pair has thus far eluded other approaches.

DOI: 10.1103/PhysRevA.85.062317 PACS number(s): 03.67.Bg, 42.65.Lm, 03.67.Mn

I. INTRODUCTION

Most breakthroughs in photonic realizations of quantum information processing (QIP), such as quantum teleportation [1,2], quantum cryptography [3–5], and quantum computation [6–8], have made use of the two-dimensional (2D) qubit Hilbert space of photon polarization. Entangled two-photon states produced by optical spontaneous parametric down-conversion (SPDC) from a nonlinear crystal (NLC) [9–14] have served as the workhorse of these demonstrations. Further advancement of photonic QIP is predicated on producing states in larger Hilbert spaces [15,16]. One path to increasing the size of the Hilbert space is via production of N-photon states (e.g., $N = 4$ [17], $N = 6$ [18], and $N = 8$ [19]). Pursuit of this strategy is hampered by fundamental experimental difficulties. Since the SPDC conversion efficiency is very low, generating multiple photon pairs requires high-power ultrafast pump lasers and is currently limited by the optical damage threshold in available NLCs. Moreover, restrictions on linear transformations of multiphoton states in the absence of photon-photon interactions limit the space of accessible states. In light of these difficulties, we restrict ourselves in this paper to *two-photon* states, $N = 2$, which are readily produced by SPDC.

Instead of increasing the number of photons occupying the quantum state, one may alternatively encode *qudits* or *multiple qubits per photon*. The large-dimensional Hilbert space corresponding to the spatial degree of freedom (DOF) of a photon [20] is therefore an attractive candidate for QIP [21] and quantum metrology [22]. Nevertheless, until recently [23–25], there have been no demonstrations of the direct encoding *and* manipulation of spatial quantum information without recourse to truncating the Hilbert space by spatial or modal filtering. Previous attempts include using (i) distinct optical paths [26], (ii) pixellated spatial domains [27–31], and (iii) orbital angular momentum (OAM) states [32].

The first approach to encoding quantum information in a spatial DOF relied on selecting discrete directions (i.e., linear momentum states) [26]. In this conception, two spatially filtered, well-separated directions or optical paths constitute a qubit. Theoretical studies have shown that utilizing N spatial paths and two-port beam splitters may be used to implement an arbitrary N-port unitary operator [33,34]. This spatial realization of quantum information is not easily scalable to larger Hilbert spaces, since the demands on phase stability grow exponentially with the number of optical paths selected. Experimental progress along this route has made use of fiber multiports [35], free-space longitudinal momentum-state filtering [36], and on-chip coupled waveguides [37].

A second approach to encoding quantum information in the spatial DOF is to discretize the transverse plane into mutually exclusive patches, or "pixels," that correspond to orthogonal functions taken as the basis of a Hilbert space. This approach was used by Walborn *et al*. [31] to implement a single-photon, large-alphabet quantum key distribution protocol and was also applied to entangled photon pairs [29,30]. Although such a scheme is feasible in principle, it is difficult to construct unitary operators on this Hilbert space. Fourier-transform (FT) systems and imaging systems (a cascade of two FT systems [38]) were used to implement "rotations" in the pixellated Hilbert space [29–31]. It is now understood from research on the fractional FT [39,40] that the FT is in fact a rotation in the position-momentum space of the Wigner function associated with the field and *not* in the Hilbert space constructed on the spatial domain [41]. This fact casts doubt on the potential of simple pixellation schemes as a route to spatial-domain QIP.

A third approach is the use of the rotational DOF of OAM [42,43]. Pairs of photons produced by SPDC are in fact described by a large-dimensional entangled-OAM state [32] whose bandwidth has now been measured [44]. A recent experiment on generalized-Bell-inequality violation infers the existence of a high-dimensional OAM-entangled state [45]. Nevertheless, direct manipulation of photon-pair OAM states

*raddy@creol.ucf.edu
†Currently with Massachusetts Institute of Technology, Lincoln Laboratory, Lexington, MA 02420, USA.

has thus far been limited to a low-dimensional Hilbert space per photon through modal filtering [32,46,47].

Further increase in the information-carrying capacity of a photon is achieved by utilizing multiple DOFs simultaneously. When two photons are entangled in each of multiple DOFs separately, they are said to be "hyperentangled" [48–52]. Hyperentangled multiqubit states have been characterized via quantum-state tomography [52], used to implement deterministic two-qubit single-photon gates [27,28], to test the foundations of quantum mechanics [53–57], and in cluster-state one-way quantum computation [58,59]. Nevertheless, the experimental complexity for the simultaneous manipulation of different physical DOFs is daunting.

We recently introduced an approach for encoding quantum information in photonic states using a global *spatial* property of a photon, namely, its *spatial parity* along one dimension (1D) [23,25]. The central insight that led to this approach was the recognition of the isomorphism between *single-mode multiphoton* states and *single-photon multimode* states of the electromagnetic field [23]. Previous theoretical proposals [60–62] for violating Bell's inequality [63] using the Einstein-Podolsky-Rosen (EPR) state [64] relied on casting that state in a multiphoton Fock basis. Such states are not feasibly produced using current or foreseeable technology. Our insight in Ref. [23] allows one to translate the proposed *single*-mode *multi*-photon states into readily produced *multi*-mode *single*-photon states. This led to experimental demonstrations of the controlled preparation of entangled 1D spatial-parity qubits using SPDC photon pairs [25] and the first violation of Bell's inequality using the EPR state [24]. Subsequent work on OAM benefited from these developments, leading to an analogous violation of Bell's inequality [65,66].

In this paper, we extend our one- and two-photon 1D spatial-parity formulation into a 2D Cartesian space. While this is a simple extension to realize experimentally, we find that this *nontrivial conceptual extension* allows one to encode *two logical qubits in a single-photon transverse spatial field*. Each qubit may be manipulated via unitary transformations and projected onto a basis using simple linear optical components. Moreover, the two qubits encoded in a single photon may be jointly rotated in their combined Hilbert space, resulting in nonseparable, one-photon, two-qubit states. An *arbitrary one-photon, two-qubit state* is prepared by modulating the field transverse spatial distribution. Moreover, we demonstrate that photon pairs produced by SPDC enable the encoding of *four* entangled logical qubits, two in each photon. We describe how *arbitrary two-photon, four-qubit states* may be prepared, and the associated 16-dimensional Hilbert space spanned, by sculpting the phase and amplitude of the classical optical pump used in the SPDC process. We highlight the capabilities of this approach by describing the preparation of two classes of four-qubit states that have heretofore eluded realization using photon pairs: a four-qubit Greenberger-Horne-Zeilinger (GHZ) state and a four-qubit W state. Our approach owes its experimental simplicity to the fact that the two qubits per photon are carried in the photon global spatial profile and manipulation of the beam profile engenders the qubit transformations, allowing for simple cascading of multiple operations.

We highlight an important distinction between our approach and that of OAM. In the polar-coordinate system appropriate for OAM, the radial r and angular θ coordinates are asymmetric from a geometric standpoint. While the angular modes have been the focus of attention to date, schemes developed for manipulating OAM are not suitable for manipulating the radial modes. The radial DOF has consequently been ignored in all OAM schemes used for QIP (see recent exceptions that consider radial OAM modes [67,68]). In contrast to the *asymmetry* between r and θ in polar coordinates, our approach utilizes the parity in the orthogonal x and y Cartesian coordinates, which are intrinsically *symmetric*. Thus, the devices developed to manipulate 1D spatial parity along x in Refs. [23–25,69] can also be used for manipulating the y parity after an appropriate rotation. Furthermore, we demonstrate in this paper that simple optical devices controllably *couple* or *correlate* parity in x and y by operating in their joint Hilbert space.

The paper is organized as follows. We first review the elements of one- and two-photon spatial parity in 1D. Next, we introduce the concept of one-photon 2D spatial parity in x and y, and then extend the formalism to two-photon states. An Appendix describes the SPDC state used. For convenience, we use the following abbreviations throughout the paper: 1P (one-photon), 2P (two-photon), 1P-1D (one photon, one-dimensional parity), etc. We also use "parity" for "spatial parity" throughout for brevity.

II. ONE-PHOTON ONE-DIMENSIONAL (1P-1D) PARITY SPACE

We first offer, for completeness, a description of 1D parity for a 1P state (1P-1D hereafter). Our presentation is simpler than that in Ref. [23] and lays the groundwork for our subsequent generalization to 2D parity. Consider a pure 1P state, $|\Psi\rangle = \int dx\, \psi(x)|1_x\rangle$, where $\langle\Psi|\Psi\rangle = 1$ implies that $\int dx|\psi(x)|^2 = 1$, and x is a 1D transverse Cartesian spatial coordinate. We assume that the field spatial distribution is separable in x and y and we trace over the y dependence. We focus on state functions having the form

$$\psi(x) = \varphi(x)\{\alpha u_0(x) + \beta u_1(x)\}, \tag{1}$$

where $u_0(x)$ and the Heaviside step function $u_1(x)$ are even and odd functions, respectively [Fig. 1(a)], $\varphi(x)$ is a generic even function normalized such that $\int dx|\varphi(x)|^2 = 1$, and $|\alpha|^2 + |\beta|^2 = 1$. We construct a 2D (qubit) Hilbert space for 1P-1D parity by identifying the logical basis $\{|0\rangle,|1\rangle\}$ with the orthogonal functions $u_0(x)$ and $u_1(x)$. In this Hilbert space, the state function in Eq. (1) corresponds to the qubit state

$$|\Psi\rangle = \alpha|0\rangle + \beta|1\rangle. \tag{2}$$

We thus establish a *mapping* from the space of *spatial photon field distributions* in Eq. (1) to the space of *logical qubit states* in Eq. (2).

To prepare an *arbitrary* qubit, we need only control the relative amplitude and phase of the two halves of the 1P field along x. Writing $\alpha = \cos\frac{\theta}{2}$ and $\beta = \sin\frac{\theta}{2}e^{i\phi}$, we identify a case of particular interest when $\phi = \frac{\pi}{2}$, whereupon $|\Psi\rangle = \cos\frac{\theta}{2}|0\rangle + i\sin\frac{\theta}{2}|1\rangle$. Since $\cos\{\frac{\theta}{2}u_1(x)\} = \cos\frac{\theta}{2}u_0(x)$ and $\sin\{\frac{\theta}{2}u_1(x)\} = \sin\frac{\theta}{2}u_1(x)$, the corresponding state func-

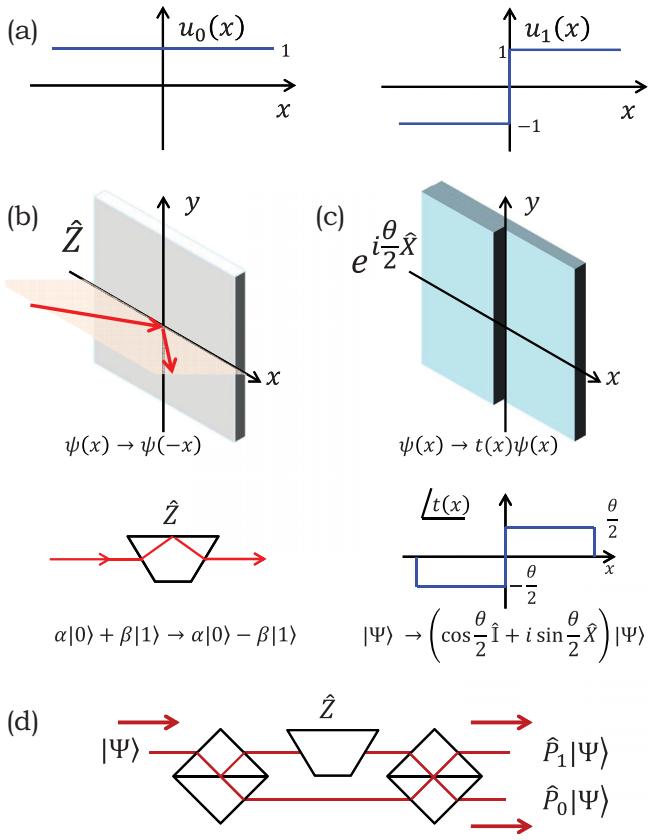

FIG. 1. (Color online) 1D parity qubits and operators on 1D parity space. (a) The basis functions $u_0(x)$ and $u_1(x)$, (b) a realization of a spatial flipper corresponding to the $\hat{Z}$ operator and its symbolic representation, (c) a spatial parity rotator $\hat{R}_x(\theta) = e^{i\frac{\theta}{2}\hat{X}}$ implemented using a phase plate with phase θ between the two halves [$\hat{R}_x(\pi) = i\hat{X}$], and (d) a parity analyzer $\frac{1}{2}\{\hat{\mathbb{I}} \pm \hat{Z}\}$ for 1D parity qubits realized using a balanced MZI with the $\hat{Z}$ parity operator in one arm. $\psi(x)$ is the 1D spatial state function; $t(x)$ is the spatial distribution impressed upon the optical field, a pure phase here.

tion is then

$$\psi(x) = \varphi(x)\exp\left\{i\frac{\theta}{2}u_1(x)\right\}, \tag{3}$$

and the amplitude of the state function $|\psi(x)| = |\varphi(x)|$ is independent of θ. The information is thus encoded solely in the *phase* of the 1P field and transformations among states in this class may be implemented by spatial phase modulation alone.

We next identify optical systems that implement spatial transformations that are closed on the class of states described in Eq. (1). Such transformations are described either by an impulse response function in the *spatial* representation or a 2×2 matrix operator in the *parity* representation. In the spatial representation, a linear device transforms the state function $\psi(x)$ to $\psi'(x) = \int dx' h(x,x')\psi(x')$, where $h(x,x')$ is the impulse response function [70]. We consider here devices having $h(x,x') = t(x)\delta(x \mp x')$; i.e., $\psi(x)$ is modulated by $t(x)$ and may also be reflected around the origin. Note that h is unitary if $t(x)$ is a unit-amplitude phase function, $t(x) = \exp\{i\theta(x)\}$. We introduce two optical devices in Figs. 1(b) and 1(c) whose actions on 1P-1D parity correspond to the Pauli operators $\hat{Z}$ and $\hat{X}$. The $\hat{Z}$ parity operator [Fig. 1(b)] performs the transformation $|0\rangle \to |0\rangle$ and $|1\rangle \to -|1\rangle$, or $u_0(x) \to u_0(x)$ and $u_1(x) \to -u_1(x)$ in the spatial representation. This is achieved by a spatial reflection (spatial flip) around the origin, $h(x,x') = \delta(x + x')$, which may be implemented using a mirror or a dove prism [23]. The $\hat{X}$ parity operator performs the transformation $|0\rangle \to |1\rangle$ and $|1\rangle \to |0\rangle$, or $u_0(x) \to u_1(x)$ and $u_1(x) \to u_0(x)$ in the spatial representation, and is implemented using a phase plate or a spatial light modulator (SLM) with a π-phase shift between the two halves of the plane, $h(x,x') = u_1(x)\delta(x - x')$ [Fig. 1(c) with θ set to π].

Using the $\hat{X}$ and $\hat{Z}$ parity operators, we construct two important operators. The first is a parity *rotation* operator

$$\hat{R}_x(\theta) = e^{i\frac{\theta}{2}\hat{X}} = \cos\frac{\theta}{2}\hat{\mathbb{I}} + i\sin\frac{\theta}{2}\hat{X} = \begin{pmatrix} \cos\frac{\theta}{2} & i\sin\frac{\theta}{2} \\ i\sin\frac{\theta}{2} & \cos\frac{\theta}{2} \end{pmatrix}, \tag{4}$$

which rotates the 1D parity state an angle θ around a major circle on a parity Poincaré sphere [25], with $\hat{R}_x(\pi) = i\hat{X}$. Thus starting from the fiducial state $|\Psi\rangle = |0\rangle$, $\psi(x) = \varphi(x)$, $\hat{R}_x(\theta)$ produces the state $|\Psi\rangle = \cos\frac{\theta}{2}|0\rangle + i\sin\frac{\theta}{2}|1\rangle$. In the spatial representation, this operator corresponds to an optical system having $h(x,x') = e^{i\frac{\theta}{2}u_1(x)}\delta(x - x')$ implemented using a phase plate or SLM having a constant phase in each half plane and a phase difference θ between the two halves [Fig. 1(c)]. Note that this transformation affects only the phase of the state function in Eq. (3), and the class of such states thus remains closed under its action.

The second operator we construct is the parity *projection* operator $\hat{P}_0 = \frac{1}{2}\{\hat{\mathbb{I}} + \hat{Z}\} = |0\rangle\langle 0|$ and its complement $\hat{P}_1 = \frac{1}{2}\{\hat{\mathbb{I}} - \hat{Z}\} = |1\rangle\langle 1| = \hat{\mathbb{I}} - \hat{P}_0$ in the even-odd basis. In the spatial representation, $\hat{P}_0$ and $\hat{P}_1$ correspond to the transformations $\psi(x) \to \frac{1}{2}\{\psi(x) + \psi(-x)\}$ and $\psi(x) \to \frac{1}{2}\{\psi(x) - \psi(-x)\}$, respectively, implemented using a *balanced* Mach-Zehnder interferometer (MZI) with a spatial flip $\hat{Z}$ in one of its arms [Fig. 1(d)]. No temporal scanning is needed in this modified MZI.

Bringing all the above-described elements together, as summarized in Table I, coherent control over the Hilbert space of 1P-1D x-parity states is enabled. The class of state functions having the form of Eq. (1) is closed under the parity transformations we consider here. Although we have presented the formalism of 1D parity using the x spatial

TABLE I. The spatial representation of a 1P-1D parity state and the corresponding logical-qubit representation.

Spatial representation	Logical qubit
$\varphi(x)u_0(x)$, even	$\|0\rangle$
$\varphi(x)u_1(x)$, odd	$\|1\rangle$
$\psi(x) = \varphi(x)\{\alpha u_0(x) + \beta u_1(x)\}$	$\|\Psi\rangle = \alpha\|0\rangle + \beta\|1\rangle$
$\psi(x) \to \psi(-x)$	$\|\Psi\rangle \to \hat{Z}\|\Psi\rangle$
$\psi(x) \to u_1(x)\psi(x)$	$\|\Psi\rangle \to \hat{X}\|\Psi\rangle$
$\psi(x) \to e^{i\frac{\theta}{2}u_1(x)}\psi(x)$	$\|\Psi\rangle \to \hat{R}_x(\theta)\|\Psi\rangle$
$\psi(x) \to \frac{1}{2}\{\psi(x) + \psi(-x)\}$	$\|\Psi\rangle \to \hat{P}_0\|\Psi\rangle = \|0\rangle\langle 0\|\Psi\rangle$
$\psi(x) \to \frac{1}{2}\{\psi(x) - \psi(-x)\}$	$\|\Psi\rangle \to \hat{P}_1\|\Psi\rangle = \|1\rangle\langle 1\|\Psi\rangle$

parameter while tracing over y, it should be clear that this approach may be also applied to the y spatial parameter after tracing over x. Taking the two spatial dimensions together, new possibilities for information encoding are enabled, as we show subsequently.

III. TWO-PHOTON ONE-DIMENSIONAL (2P-1D) PARITY SPACE

Consider a general pure 2P state where each photon is described by a 1D spatial parameter after tracing over the second coordinate of each photon:

$$|\Psi\rangle = \iint dx dx' \psi(x,x') |1_x, 1_{x'}\rangle, \tag{5}$$

where the state function $\psi(x,x')$ is normalized such that $\iint dx dx' |\psi(x,x')|^2 = 1$ [14]. Using SPDC to generate photon pairs [Fig. 2(a)], $\psi(x,x')$ is determined by the parameters of the classical optical pump and the NLC. By judicious design of these parameters we can encode *an arbitrary two-qubit parity state* in the photon pair. Using the conditions outlined in the Appendix (type I, collinear, spectrally narrow band, degenerate SPDC from a thin NLC), the state function may be approximated by

$$\psi(x,x') \approx E_{\rm p}(x)\delta(x - x'), \tag{6}$$

where $E_{\rm p}(x)$ is the spatial profile of the classical optical pump in 1D. If $E_{\rm p}$ is even, $E_{\rm p}(x) = \varphi(x)u_0(x) = E_{\rm p}(-x)$, it can be shown [23] that the resulting entangled 2P-1D parity state corresponds in parity space to the two-qubit Bell state $|\Phi^+\rangle = \frac{1}{\sqrt{2}}\{|00\rangle + |11\rangle\}$; i.e., if the pump has even parity, then both photons have the same parity (both have even parity or both have odd parity). On the other hand, if the pump is odd $E_{\rm p}(x) = \varphi(x)u_1(x) = -E_{\rm p}(-x)$, the resulting 2P-1D state is $|\Psi^+\rangle = \frac{1}{\sqrt{2}}\{|01\rangle + |10\rangle\}$; i.e., if the pump has odd parity, then the two photons have opposite parity (one of them has even parity and the other has odd parity).

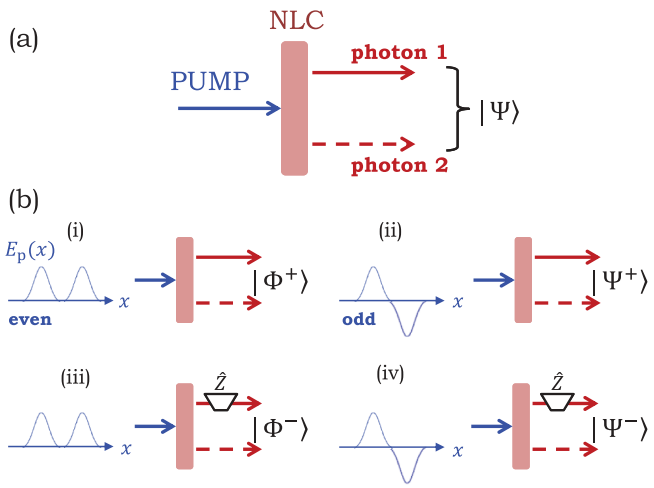

FIG. 2. (Color online) (a) A classical pump is incident on a nonlinear crystal (NLC) and generates a two-photon spatial parity state $|\Psi\rangle$. (b) Schematics of the configurations for generating the four Bell states: (i) $|\Phi^+\rangle$, an even pump; (ii) $|\Psi^+\rangle$, an odd pump; (iii) $|\Phi^-\rangle$, an even pump and a spatial flip $\hat{Z}$ in the path of one photon; and (iv) $|\Psi^-\rangle$, an odd pump and $\hat{Z}$ in the path of one photon.

Consequently, if the pump is prepared in an arbitrary parity superposition,

$$E_{\rm p}(x) = \varphi(x)\left\{\cos\frac{\theta}{2}u_0(x) + e^{i\phi}\sin\frac{\theta}{2}u_1(x)\right\}, \tag{7}$$

then the resulting 2P-1D state is

$$|\Psi\rangle = \cos\frac{\theta}{2}|\Phi^+\rangle + e^{i\phi}\sin\frac{\theta}{2}|\Psi^+\rangle, \tag{8}$$

which may or may not be entangled, according to the values of θ and ϕ. Interestingly, it is not possible to generate the Bell states $|\Phi^-\rangle$ and $|\Psi^-\rangle$ by manipulating the pump profile alone when a thin NLC is used. Further control over the 2P-1D state may be achieved by manipulating the parity of the down-converted photons. For example, when a spatial flip $\hat{Z}$ is implemented in the path of one photon of the pair, an even pump produces the $|\Phi^-\rangle$ state with corresponding state function $\psi(x,x') = \varphi(x)\delta(x + x')$, while an odd pump produces the $|\Psi^-\rangle$ state with state function $\psi(x,x') = \varphi(x)u_1(x)\delta(x + x')$. In this manner, all four Bell states are prepared, as shown schematically in Fig. 2(b).

Combining control over the classical pump profile $E_{\rm p}(x)$ and the parity of the SPDC photons, we may *span* the Hilbert space of *pure* two-qubit states. To elucidate this statement, it is most convenient to use the Bell states $\{|\Phi^+\rangle, |\Psi^+\rangle, |\Phi^-\rangle, |\Psi^-\rangle\}$ as a basis for the 2P-1D space, in which case an arbitrary two-qubit pure state is

$$\begin{aligned}|\Psi\rangle &= \alpha_1|\Phi^+\rangle + \alpha_2|\Psi^+\rangle + \alpha_3|\Phi^-\rangle + \alpha_4|\Psi^-\rangle,\\ &= \frac{\alpha_1 + \alpha_3}{\sqrt{2}}|00\rangle + \frac{\alpha_2 + \alpha_4}{\sqrt{2}}|01\rangle + \frac{\alpha_2 - \alpha_4}{\sqrt{2}}|10\rangle\\ &\quad + \frac{\alpha_1 - \alpha_3}{\sqrt{2}}|11\rangle.\end{aligned} \tag{9}$$

We prepare this state using two NLCs (NLC1 and NLC2) with pump profiles $E_{{\rm p}j}(x) = \varphi(x)\{\cos\frac{\theta_j}{2}u_0(x) + \sin\frac{\theta_j}{2}e^{i\phi_j}u_1(x)\}$, each producing the state $|\Psi_j\rangle = \cos\frac{\theta_j}{2}|\Phi^+\rangle + \sin\frac{\theta_j}{2}e^{i\phi_j}|\Psi^+\rangle$, $j = 1,2$. A spatial flip $\hat{Z}$ is placed in the path of one of the photons produced by NLC2, for example, such that $|\Psi_2\rangle = \cos\frac{\theta_2}{2}|\Phi^-\rangle + \sin\frac{\theta_2}{2}e^{i\phi_2}|\Psi^-\rangle$. The states $|\Psi_1\rangle$ and $|\Psi_2\rangle$ are then superposed to produce the state $|\Psi\rangle = \cos\frac{\theta}{2}|\Psi_1\rangle + \sin\frac{\theta}{2}e^{i\phi}|\Psi_2\rangle$. The parameters used in generating $|\Psi\rangle$ are related to the desired coefficients in Eq. (9) through the following one-to-one relationships:

$$\begin{aligned}\alpha_1 &= \cos\frac{\theta}{2}\cos\frac{\theta_1}{2}, \quad \alpha_2 = \cos\frac{\theta}{2}\sin\frac{\theta_1}{2}e^{i\phi_1},\\ \alpha_3 &= \sin\frac{\theta}{2}\cos\frac{\theta_2}{2}e^{i\phi}, \quad \alpha_4 = \sin\frac{\theta}{2}\sin\frac{\theta_2}{2}e^{i(\phi_2+\phi)}.\end{aligned}$$

The superposition parameters θ and ϕ are set by controlling the relative amplitude and phase of the two classical pumps. The photon-pair probability amplitudes are then overlapped at two identical symmetric beam splitters, as shown in Fig. 3. Only two photons are produced in this scheme by *one* of the NLCs, and the overlap at the beam splitters is between the probability

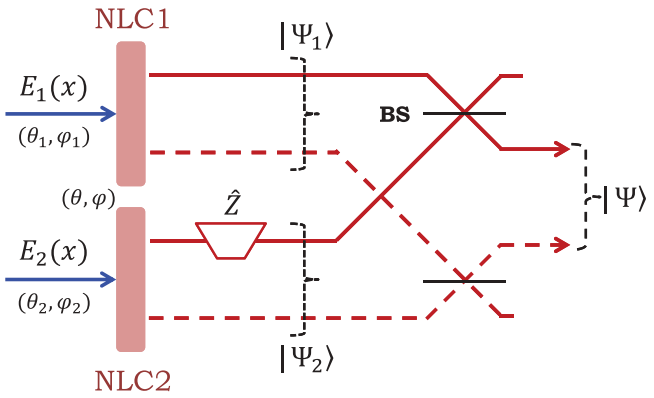

FIG. 3. (Color online) Setup for preparing a general 2P-1D parity state by superposing the states $|\Psi_1\rangle$ and $|\Psi_2\rangle$ from two NLCs pumped by mutually coherent pumps.

amplitudes of the photon pair being produced by NLC1 *or* NLC2. The state is produced after postselecting for the two photons emerging from the desired ports, which occurs 25% of the time. Using this arrangement, an *arbitrary* two-qubit state is encoded in 2P-1D parity.

We have thus established a mapping between 2P-1D state functions of the form

$$\psi(x,x') = \varphi(x)\{[\alpha_1 u_0(x) + \alpha_2 u_1(x)]\delta(x - x') + [\alpha_3 u_0(x) + \alpha_4 u_1(x)]\delta(x + x')\}, \quad (10)$$

and the logical two-qubit state in Eq. (9). Thus by sculpting the spatial distributions $E_1(x)$ and $E_2(x)$ of the pumps, by setting the values of $\alpha_1, \alpha_2, \alpha_3$, and α_4, we prepare an arbitrary two-qubit state. For example, to prepare the separable state $|00\rangle$, we set the values $\alpha_1 = \alpha_3 = \frac{1}{\sqrt{2}}$ and $\alpha_2 = \alpha_4 = 0$; i.e., both $E_1(x)$ and $E_2(x)$ are even functions of equal weight, and the state function becomes

$$\psi(x,x') = \frac{1}{\sqrt{2}}\varphi(x)\{\delta(x - x') + \delta(x + x')\}. \quad (11)$$

The two photons are then in an equal superposition of being correlated [the $\delta(x - x')$ term] or anticorrelated [the $\delta(x + x')$ term] in position. A subtle point must be made here. Although $\psi(x,x')$ in Eq. (11) *is nonseparable* in the spatial x–x' coordinate space, it *is separable* in parity space since the global symmetry of the state ensures that the two photons both have even parity.

The parity transformations described for 1P-1D states may be used with each photon in a 2P-1D state. Since the parity space of each photon is closed under the operation of the transformations described in the previous section, the 2P-1D parity space is in turn closed under these transformations operating on each photon. For example, parity rotations $\hat{R}_x(\theta)$ and projections ($\hat{P}_0$ and $\hat{P}_1$) may be placed in the path of each photon to implement a test of Bell's inequality violation [24]. The parity of the pump determines the degree of entanglement [71], or concurrence [72,73], of the 2P-1D state. This was confirmed experimentally in Ref. [24] by measuring the violation of the CHSH-Bell inequality [63,74] for different $E_p(x)$. The degree of entanglement of the state in Eq. (8) is $P = \sqrt{1 - \sin^2\theta\cos^2\phi}$. When $\phi = \pi/2$, the 2P-1D state is maximally entangled ($P = 1$) for all θ, as confirmed experimentally for $\theta = \pi/2$ [24]. Setting $\phi = 0$ instead, we have $P = |\cos\theta|$; see Ref. [24] for $\theta = 0$ and $\theta = \pi$ ($P = 1$), and $\theta = \frac{\pi}{2}$ ($P = 0$).

IV. ONE-PHOTON TWO-DIMENSIONAL PARITY SPACE (1P-2D)

We proceed to extend the 1P-1D x-parity description to include two transverse spatial dimensions, x and y. This nontrivial extension allows us to encode two parity qubits in a single photon, one in the parity of each dimension. The two qubits may be controlled *independently* or, alternatively, *coupled* to become correlated in a manner that is mathematically isomorphic to entangled two-photon states. Furthermore, since the two qubits are realized on a single photon, we may subsequently "disentangle" them.

As mentioned earlier, this symmetry between x and y is in contrast to the asymmetry between the radial and angular coordinates, r and θ, respectively, in a polar-coordinate system. The angular dimension is manipulated to encode information in OAM states while the orthogonal radial dimension is typically ignored. In contrast, in our formulation both x and y parity qubits are brought under control using the same optical devices. We proceed to describe the encoding, manipulation, and analysis of two qubits in 1P-2D states.

A. 1P-2D parity states

Consider a general 1P pure state with transverse Cartesian coordinates x and y,

$$|\Psi\rangle = \iint dxdy\ \psi(x,y)|1_{x,y}\rangle, \quad (12)$$

where $\iint dxdy|\psi(x,y)|^2 = 1$. By sculpting the state function $\psi(x,y)$, we may encode an arbitrary two-qubit state in the photon. Consider first a state with separable state function $\psi(x,y) = \psi_1(x)\psi_2(y)$. Both ψ_1 and ψ_2 are in the form of Eq. (1). We take this state to correspond to the logical separable two-qubit state $|\Psi\rangle = |\Psi_1\rangle_x \otimes |\Psi_2\rangle_y$, where the mapping from the spatial state functions $\psi_1(x)$ and $\psi_2(y)$ to the logical-qubit states $|\Psi_1\rangle_x$ and $|\Psi_2\rangle_y$, respectively, is the same as that in the 1P-1D case (see Table I). Therefore, in the special case $\psi_1(x) = \varphi(x)$ and $\psi_2(y) = \varphi(y)$, $\psi(x,y) = \varphi(x)\varphi(y) = u_{00}(x,y)$, we identify the state as $|\Psi\rangle = |0\rangle_x \otimes |0\rangle_y$. The state function $\psi(x,y) = \varphi(x)u_1(x)\varphi(y)u_1(y) = u_{11}(x,y)$, a product of odd functions in x and y, corresponds to the two-qubit state $|\Psi\rangle = |1\rangle_x \otimes |1\rangle_y$. Similarly, the states $|0\rangle_x \otimes |1\rangle_y$ and $|1\rangle_x \otimes |0\rangle_y$ correspond to state functions $u_{01}(x,y) = \varphi(x)u_0(x)\varphi(y)u_1(y)$ and $u_{10}(x,y) = \varphi(x)u_1(x)\varphi(y)u_0(y)$, respectively. It is understood hereafter in this section that $|00\rangle = |0\rangle_x \otimes |0\rangle_y$, and so on. Note that $|u_{00}(x,y)| = |u_{01}(x,y)| = |u_{10}(x,y)| = |u_{11}(x,y)| = |\varphi(x)||\varphi(y)|$, and the parity is encoded solely in the *phase* of each distribution. These four states establish the x-y basis for the two-qubit 1P-2D parity Hilbert space. The 2D spatial phase distributions of these basis states are shown in Fig. 4(a).

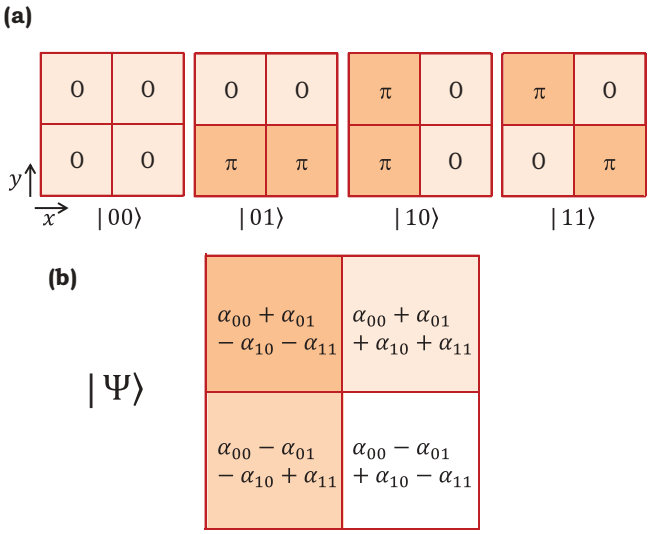

FIG. 4. (Color online) 1P-2D spatial parity qubits. (a) The *phase* distribution of the basis functions $u_{00}(x,y)$, $u_{01}(x,y)$, $u_{10}(x,y)$, and $u_{11}(x,y)$, corresponding to the states $|00\rangle$, $|01\rangle$, $|10\rangle$, and $|11\rangle$. The phase in each quadrant is constant. There is no amplitude variation needed in any of these basis states. (b) The *complex amplitude* distribution in each quadrant necessary to produce the general state $|\Psi\rangle$ given in Eq. (13). The complex amplitude is constant in each quadrant.

The most general pure state in this conception,

$$|\Psi\rangle = \alpha_{00}|00\rangle + \alpha_{01}|01\rangle + \alpha_{10}|10\rangle + \alpha_{11}|11\rangle, \qquad (13)$$

with the normalization $|\alpha_{00}|^2 + |\alpha_{01}|^2 + |\alpha_{10}|^2 + |\alpha_{11}|^2 = 1$, corresponds to the state function

$$\psi(x,y) = \alpha_{00}u_{00}(x,y) + \alpha_{01}u_{01}(x,y) + \alpha_{10}u_{10}(x,y) + \alpha_{11}u_{11}(x,y). \qquad (14)$$

We have thus established a mapping from the space of 1P-2D states having the spatial distribution in Eq. (14) to the space of two-qubit states in Eq. (13). In order to prepare this four-dimensional (six-parameter) state, we need only control the relative amplitudes and phases of the four quadrants of the x-y plane while maintaining constant amplitude and phase *within* each quadrant, as shown in Fig. 4(b). One-qubit and two-qubit transformations may be defined on 1P-2D parity space. The transformations must be constructed in such a way as to guarantee that the class of states in Eq. (14) is closed under their operation. We proceed to show that such transformations are implemented by modulating the amplitudes and phases of the four quadrants of the x-y plane.

B. Transformations on 1P-2D parity space

In this section, we describe linear optical devices that implement operations on the 1P-2D parity space. A linear optical device in the 2D *spatial* representation is described by an impulse response function $h(x,y;x',y')$ such that $\psi'(x,y) = \iint dx'dy'h(x,y;x',y')\psi(x',y')$. We consider devices where $h(x,y;x',y') = t(x,y)\delta(x \mp x')\delta(y \mp y')$. In other words, $\psi(x,y)$ is modulated by the distribution $t(x,y)$, and is also potentially flipped in x, y, or both. For a unitary transformation, $t(x,y) = \exp\{i\theta(x,y)\}$. In the 2D *parity* representation, such devices are characterized by 4×4 matrix operators.

A unique feature of this approach is that both one-qubit and two-qubit rotations are implemented in a straightforward fashion using SLMs that impart a spatially varying 2D phase distribution $\exp\{i\theta(x,y)\}$ with spatial phase distributions $\theta(x,y)$ that are constant in each of the four quadrants of the transverse plane. We described earlier how the 1P-1D parity rotation operator $\hat{R}_x(\theta) = \exp\{i\frac{\theta}{2}\hat{X}\}$ is implemented using an SLM with phase distribution $\frac{\theta}{2}u_1(x)$ and no variation along y. We now extend this approach to parity rotations in both x and y and show that these operators may also be implemented using an SLM.

We define Pauli operators on the x- and y-parity subspaces and identify them by their subscripts: $\hat{\mathbb{I}}_x$, $\hat{X}_x$, and $\hat{Z}_x$ on x, and $\hat{\mathbb{I}}_y$, $\hat{X}_y$, and $\hat{Z}_y$ on y. $\hat{X}_x$, for example, transforms x parity in the usual way while not affecting the y parity. Its impulse response function $h(x,x';y,y') = u_1(x)\delta(x-x')\delta(y-y')$, i.e., $t(x,y) = u_1(x)$, corresponds to $\hat{X}_x \otimes \hat{\mathbb{I}}_y$. The implementation of $\hat{X}_x$ and $\hat{X}_y$ differs only by a rotation of 90°, which results in an exchange of the x and y axes, leading to $h(x,y;x',y') = u_1(y)\delta(x-x')\delta(y-y')$, which corresponds to $\hat{\mathbb{I}}_x \otimes \hat{X}_y$.

1. One-qubit rotations

We first describe a one-qubit rotation operator that rotates the x-parity subspace by an angle θ. This is the same operation that we described earlier for the 1P-1D case and is implemented by the phase transformation $t(x,y;\theta) = \exp\{i\frac{\theta}{2}u_1(x)\}$ in the x-y plane [Fig. 5(a)]. The state function $\psi(x,y)$ after this transformation becomes $\exp\{i\frac{\theta}{2}u_1(x)\}\psi(x,y)$; i.e., $|\Psi\rangle \rightarrow \{\exp(i\frac{\theta}{2}\hat{X}_x) \otimes \hat{\mathbb{I}}_y\}|\Psi\rangle$. In the $\{|00\rangle,|01\rangle,|10\rangle,|11\rangle\}$ basis, the

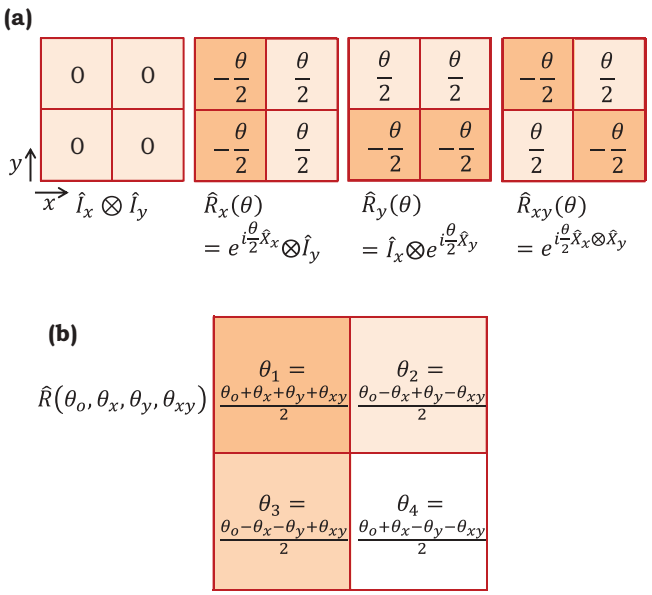

FIG. 5. (Color online) (a) Phase distribution required in implementations of one- and two-qubit 2D-parity rotations on a single photon: $\hat{\mathbb{I}}_x \otimes \hat{\mathbb{I}}_y$, $\hat{R}_x(\theta)$, $\hat{R}_y(\theta)$, and $\hat{R}_{xy}(\theta)$. (b) Phase distribution required to implement the operator $\hat{R}(\theta_o,\theta_x,\theta_y,\theta_{xy}) = e^{i\frac{\theta_o}{2}}\hat{R}_x(\theta_x)\hat{R}_y(\theta_y)\hat{R}_{xy}(\theta_{xy})$.

matrix representation of this rotation operator is

$$\hat{R}_x(\theta) = e^{i\frac{\theta}{2}\hat{X}_x} \otimes \hat{\mathbb{I}}_y = \begin{pmatrix} \cos\frac{\theta}{2} & 0 & i\sin\frac{\theta}{2} & 0 \\ 0 & \cos\frac{\theta}{2} & 0 & i\sin\frac{\theta}{2} \\ i\sin\frac{\theta}{2} & 0 & \cos\frac{\theta}{2} & 0 \\ 0 & i\sin\frac{\theta}{2} & 0 & \cos\frac{\theta}{2} \end{pmatrix}. \quad (15)$$

The symmetry between x and y allows us to define a one-qubit rotation operator that operates on the y-parity subspace. The phase transformation $t(x,y;\theta) = \exp\{i\frac{\theta}{2}u_1(y)\}$ that implements a phase shift θ between the two halves of the x-y plane around the x axis, i.e., along the y axis [Fig. 5(a)], corresponds to a rotation θ in the y-parity subspace and does not affect the x parity; i.e., $|\Psi\rangle \rightarrow \{\hat{\mathbb{I}}_x \otimes \exp(i\frac{\theta}{2}\hat{X}_y)\}|\Psi\rangle$. The matrix representation of this rotation operator is

$$\hat{R}_y(\theta) = \hat{\mathbb{I}}_x \otimes e^{i\frac{\theta}{2}\hat{X}_y} = \begin{pmatrix} \cos\frac{\theta}{2} & i\sin\frac{\theta}{2} & 0 & 0 \\ i\sin\frac{\theta}{2} & \cos\frac{\theta}{2} & 0 & 0 \\ 0 & 0 & \cos\frac{\theta}{2} & i\sin\frac{\theta}{2} \\ 0 & 0 & i\sin\frac{\theta}{2} & \cos\frac{\theta}{2} \end{pmatrix}. \quad (16)$$

Since $\hat{R}_x$ and $\hat{R}_y$ commute, these two operators and their products may be implemented using a single SLM. For example, implementing the operator $\hat{R}_x(\theta_1)\hat{R}_y(\theta_2) = \exp(i\frac{\theta_1}{2}\hat{X}_x) \otimes \exp(i\frac{\theta_2}{2}\hat{X}_y)$ requires that the phase on the SLM take the form $\frac{1}{2}\{\theta_1 u_1(x) + \theta_2 u_1(y)\}$. This is achieved with an SLM imparting the constant phases $\frac{1}{2}(\theta_1+\theta_2)$, $\frac{1}{2}(-\theta_1+\theta_2)$, $\frac{1}{2}(-\theta_1-\theta_2)$, and $\frac{1}{2}(\theta_1-\theta_2)$ to the four quadrants of the optical field in the x-y plane (taken in counterclockwise order).

2. Two-qubit rotations

We now introduce a two-qubit "parity-entangling" operator that operates on the joint Hilbert space of x and y parity. This operator rotates x-y parity by an angle θ, resulting in the coupling of parity in x-y starting from an initially separable state. Consider the phase transformation $t(x,y;\theta) = \exp\{i\frac{\theta}{2}u_1(x)u_1(y)\}$, which is nonseparable in x and y, and thus couples the x and y parities. This transformation may be implemented with an SLM with constant phases $\frac{\theta}{2}$, $-\frac{\theta}{2}$, $\frac{\theta}{2}$, and $-\frac{\theta}{2}$ in the four quadrants (taken in counterclockwise order), as shown in Fig. 5(a). The 1P-2D state $|\Psi\rangle$ after this transformation is $\exp\{i\frac{\theta}{2}\hat{X}_x \otimes \hat{X}_y\}|\Psi\rangle$, and the corresponding two-qubit rotation operator is

$$\hat{R}_{xy}(\theta) = \begin{pmatrix} \cos\frac{\theta}{2} & 0 & 0 & i\sin\frac{\theta}{2} \\ 0 & \cos\frac{\theta}{2} & i\sin\frac{\theta}{2} & 0 \\ 0 & i\sin\frac{\theta}{2} & \cos\frac{\theta}{2} & 0 \\ i\sin\frac{\theta}{2} & 0 & 0 & \cos\frac{\theta}{2} \end{pmatrix}. \quad (17)$$

Starting from the separable state $|\Psi\rangle = |00\rangle$, this operator produces the entangled state $\hat{R}_{xy}(\theta)|\Psi\rangle = \cos\frac{\theta}{2}|00\rangle + i\sin\frac{\theta}{2}|11\rangle$ with controllable degree of entanglement $P = |\sin\theta|$. The two Bell states $|\Phi^+\rangle$ and $|\Phi^-\rangle$ (except for the relative $\frac{\pi}{2}$ phase) are produced from $|00\rangle$ via the operators $\hat{R}_{xy}(\frac{\pi}{2})$ and $\hat{R}_{xy}(-\frac{\pi}{2})$, respectively. Starting, instead, from the separable state $|\Psi\rangle = |01\rangle$, $\hat{R}_{xy}(\theta)$ produces the entangled state $\cos\frac{\theta}{2}|01\rangle + i\sin\frac{\theta}{2}|10\rangle$. The two Bell states $|\Psi^+\rangle$ and $|\Psi^-\rangle$ are thus produced from $|01\rangle$ via the operators $\hat{R}_{xy}(\frac{\pi}{2})$ and $\hat{R}_{xy}(-\frac{\pi}{2})$, respectively. Furthermore, the inverse of $\hat{R}_{xy}(\theta)$ is $\hat{R}_{xy}(-\theta)$. Thus after $\hat{R}_{xy}(\theta)$ *entangles* the separable state $|00\rangle$, the operator $\hat{R}_{xy}(-\theta)$ *disentangles* the resulting state and returns it to the initial separable state.

These three operators, $\hat{R}_x$, $\hat{R}_y$, and $\hat{R}_{xy}$, all commute, and hence products of these operators are implementable on a single SLM.

3. General two-qubit rotations

Finally, consider the general phase transformation shown in Fig. 5(b) with constant phases θ_1, θ_2, θ_3, and θ_4 in the four quadrants. The corresponding operator may be cast as a product of four simpler commuting operators: $\hat{R}_x(\theta_x)$, $\hat{R}_y(\theta_y)$, $\hat{R}_{xy}(\theta_{xy})$, and an overall phase $\exp(i\frac{\theta_o}{2})\hat{\mathbb{I}}_x \otimes \hat{\mathbb{I}}_y$:

$$\hat{R}(\theta_o,\theta_x,\theta_y,\theta_{xy}) = e^{i\frac{\theta_o}{2}}\hat{R}_x(\theta_x)\hat{R}_y(\theta_y)\hat{R}_{xy}(\theta_{xy}). \quad (18)$$

The 1P-2D parity rotation angles θ_o, θ_x, θ_y, and θ_{xy} are related to the quadrant phases θ_1, θ_2, θ_3, and θ_4 as follows:

$$\begin{aligned} 2\theta_1 &= \theta_o + \theta_x + \theta_y + \theta_{xy}, \\ 2\theta_2 &= \theta_o - \theta_x + \theta_y - \theta_{xy}, \\ 2\theta_3 &= \theta_o - \theta_x - \theta_y + \theta_{xy}, \\ 2\theta_4 &= \theta_o + \theta_x - \theta_y - \theta_{xy}. \end{aligned} \quad (19)$$

For example, starting from $|\Psi\rangle = |00\rangle$ we can prepare $|\Psi^+\rangle$ using $\hat{R}_x(\pi)\hat{R}_{xy}(-\frac{\pi}{2})$; $\theta_1 = \frac{\pi}{4}$, $\theta_2 = -\frac{\pi}{4}$, $\theta_3 = -\frac{3\pi}{4}$, and $\theta_4 = \frac{3\pi}{4}$.

4. One- and two-qubit $\hat{Z}$ operators

We define two Pauli $\hat{Z}$ operators, $\hat{Z}_x$ and $\hat{Z}_y$, which operate on the x- and y-parity subspaces, respectively [see Figs. 6(a) and 6(b)]. The operator $\hat{Z}_x$ flips the state function along x without affecting y [Fig. 6(a)], $\psi(x,y) \rightarrow \psi(-x,y)$, corresponding to $|\Psi\rangle \rightarrow (\hat{Z}_x \otimes \hat{\mathbb{I}}_y)|\Psi\rangle$. The operator $\hat{Z}_y$ flips the state function along y, $\psi(x,y) = \psi(x,-y)$, corresponding to $|\Psi\rangle \rightarrow (\hat{\mathbb{I}}_x \otimes \hat{Z}_y)|\Psi\rangle$. The two operators may be combined, resulting in a reflection through the origin, $\psi(x,y) \rightarrow \psi(-x,-y)$, corresponding to $|\Psi\rangle \rightarrow (\hat{Z}_x \otimes \hat{Z}_y)|\Psi\rangle$. The matrix representations of these operators are

$$\underbrace{\begin{pmatrix} 1 & 0 & 0 & 0 \\ 0 & 1 & 0 & 0 \\ 0 & 0 & -1 & 0 \\ 0 & 0 & 0 & -1 \end{pmatrix}}_{\hat{Z}_x\otimes\hat{\mathbb{I}}_y}, \quad \underbrace{\begin{pmatrix} 1 & 0 & 0 & 0 \\ 0 & -1 & 0 & 0 \\ 0 & 0 & 1 & 0 \\ 0 & 0 & 0 & -1 \end{pmatrix}}_{\hat{\mathbb{I}}_x\otimes\hat{Z}_y}, \quad \underbrace{\begin{pmatrix} 1 & 0 & 0 & 0 \\ 0 & -1 & 0 & 0 \\ 0 & 0 & -1 & 0 \\ 0 & 0 & 0 & 1 \end{pmatrix}}_{\hat{Z}_x\otimes\hat{Z}_y}. \quad (20)$$

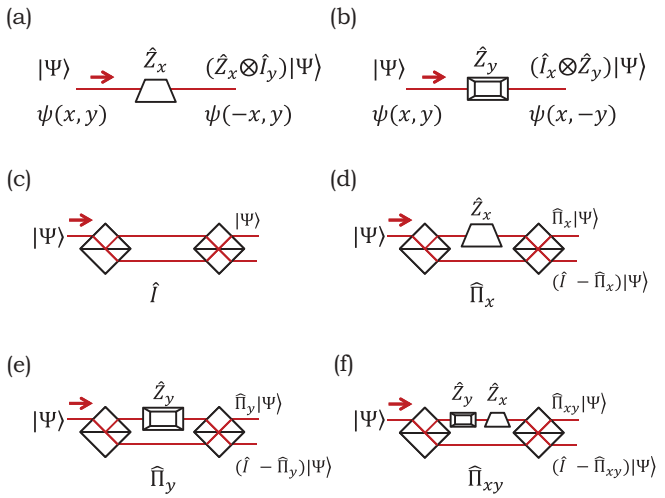

FIG. 6. (Color online) Representation of Pauli (a) $\hat{Z}_x$ and (b) $\hat{Z}_y$ operators depicted as Dove prisms oriented to perform spatial flips in x and y, respectively. (c)–(f) Representations of modified MZIs that correspond to the projection operators (c) $\hat{\mathbb{I}}_x \otimes \hat{\mathbb{I}}_y$, (d) $\hat{Z}_x \otimes \hat{\mathbb{I}}_y$, (e) $\hat{\mathbb{I}}_x \otimes \hat{Z}_y$, and (f) $\hat{Z}_x \otimes \hat{Z}_y$. The second output port of the MZIs corresponds to the orthogonal projections.

Since the operators $\hat{X}_x$ and $\hat{Z}_x$ ($\hat{X}_y$ and $\hat{Z}_y$) do not commute, the order in which rotations and spatial flips are implemented is important. We emphasize the simplicity of implementing this scheme with linear optics. Using products of rotations $\hat{X}$ and $\hat{Z}$, implemented with cascaded phase plates and spatial flips (implemented by mirrors or Dove prisms), respectively, two-qubit unitary operators on 1P-2D parity space are realized.

C. Projections on 1P-2D parity state space

We describe here the implementation of two-qubit projections on the 1P-2D parity space. The goal is to construct an arrangement that yields the weights $|\alpha_{00}|^2$, $|\alpha_{01}|^2$, $|\alpha_{10}|^2$, and $|\alpha_{11}|^2$ of the two-photon state in Eq. (13). We use a modified balanced MZI similar to that used in the 1P-1D parity case [Fig. 1(d)], with each of the following elements placed in one arm: (1) a spatial flip along x, $\hat{Z}_x \otimes \hat{\mathbb{I}}_y$; (2) a spatial flip along y, $\hat{\mathbb{I}}_x \otimes \hat{Z}_y$; and (3) a spatial flip along both x and y, $\hat{Z}_x \hat{Z}_y$ [see Figs. 6(d) and 6(f)].

These three projections correspond to the operators

$$\begin{aligned} \hat{\Pi}_x &= |00\rangle\langle 00| + |01\rangle\langle 01|, \\ \hat{\Pi}_y &= |00\rangle\langle 00| + |10\rangle\langle 10|, \\ \hat{\Pi}_{xy} &= |00\rangle\langle 00| + |11\rangle\langle 11|. \end{aligned} \tag{21}$$

The other output port of the MZI provides the complementary projections $\{\hat{\mathbb{I}} - \hat{\Pi}_t\}|\Psi\rangle$, $t = x$, y, and xy. $\hat{\Pi}_x$ and $\hat{\mathbb{I}} - \hat{\Pi}_x$ project the state according to the x parity, i.e., the photon emerges from one port if it is even along x and from the other if it is odd, regardless of the parity along y [Fig. 6(d)]; $\hat{\Pi}_y$ and $\hat{\mathbb{I}} - \hat{\Pi}_y$ project the state according to the y parity, regardless of x parity [Fig. 6(e)]; and $\hat{\Pi}_{xy}$ and $\hat{\mathbb{I}} - \hat{\Pi}_{xy}$ project the state into equal-xy-parity and opposite-xy-parity subspaces [Fig. 6(f)]—the photon emerges from one port if it is even or odd in *both* x and y, and emerges from the other port if the x parity is different from the y parity. The detection probabilities at the outputs of $\hat{\mathbb{I}}$ [Fig. 6(c)], $\hat{\Pi}_x$, $\hat{\Pi}_y$, and $\hat{\Pi}_{xy}$, are M_o, M_x, M_y, and M_{xy}, respectively, where

$$\begin{aligned} M_o &= |\alpha_{00}|^2 + |\alpha_{01}|^2 + |\alpha_{10}|^2 + |\alpha_{11}|^2, \\ M_x &= |\alpha_{00}|^2 + |\alpha_{01}|^2, \\ M_y &= |\alpha_{00}|^2 + |\alpha_{10}|^2, \\ M_{xy} &= |\alpha_{00}|^2 + |\alpha_{11}|^2. \end{aligned} \tag{22}$$

The lengths of the projections of the 1P-2D state along the basis vectors in the computational basis are

$$\begin{aligned} 2|\alpha_{00}|^2 &= -M_o + M_x + M_y + M_{xy}, \\ 2|\alpha_{01}|^2 &= M_o + M_x - M_y - M_{xy}, \\ 2|\alpha_{10}|^2 &= M_o - M_x + M_y - M_{xy}, \\ 2|\alpha_{11}|^2 &= M_o - M_x - M_y + M_{xy}. \end{aligned} \tag{23}$$

We have thus outlined the ingredients for QIP using the two-qubit state encoded in 1P-2D parity and proceed to extend this approach to 2P states.

D. Comparison between 1P-2D and 2P-1D two-qubit parity states

Both the 2P-1D and 1P-2D parity states encode two qubits. Nevertheless, there is a fundamental distinction between them. In the 2P-1D case, each qubit is realized on a single photon and may thus also be measured independently of the other. On the other hand, in the 1P-2D case, both qubits are encoded in the same photon and thus must be measured together. Moreover, the two qubits in the 1P-2D case may be easily entangled or disentangled; in other words, they may be made to "interact" using transformations that couple x and y parity. This is not straightforward in the 2P-1D case without bringing the two photons together. In the absence of photon-photon interactions, it is difficult to implement deterministic transformations on two qubits encoded on two photons, but it is feasible when they are encoded on one photon.

V. TWO-PHOTON TWO-DIMENSIONAL PARITY SPACE (2P-2D)

We now consider the general case of an entangled photon *pair* with *both* the x and y spatial dimensions retained, namely, 2P-2D parity states. Since each photon in the pair encodes two logical qubits in the x and y parity, the 2P-2D state encodes four qubits. The general 2P-2D pure state in the spatial representation is

$$|\Psi\rangle = \iint dx dx' dy dy' \, \psi(x,y;x',y') |1_{x,y}, 1_{x',y'}\rangle, \tag{24}$$

where (x,y) and (x',y') are the transverse Cartesian coordinates of each photon, and $\iint dx dx' dy dy' |\psi(x,y;x',y')|^2 = 1$. The two-photon state produced by SPDC, within the approximations outlined in the Appendix, has the state function

$$\psi(x,y;x',y') \approx E_{\mathrm{p}}(x,y)\delta(x-x')\delta(y-y'), \tag{25}$$

where $E_{\mathrm{p}}(x,y)$ is the 2D spatial profile of the classical optical pump. The state function indicates that the two photons

are produced at the same point in the x-y plane, limited by the spatial extent and profile of the pump. We proceed to describe a mapping from the 2P-2D state to a logical four-qubit space and indicate how sculpting the classical pump profile enables spanning this 16-dimensional space.

A. Mapping the SPDC 2P-2D parity state to a four-qubit space

Consider first a pump spatial profile that is separable in x and y, $E_p(x,y) = E_x(x)E_y(y)$. The 2P-2D state function in Eq. (25) may then be factorized in (x,x') and (y,y'):

$$\begin{aligned}\psi(x,y;x',y') &= \psi_1(x,x')\psi_2(y,y') \\ &= E_1(x)\delta(x-x')E_2(y)\delta(y-y'). \quad (26)\end{aligned}$$

Both terms in x and y, $E_x(x)\delta(x-x')$ and $E_y(y)\delta(y-y')$, respectively, correspond to the state functions for 2P-1D parity states that encode two qubits. The 2P-2D parity state produced by a separable pump thus separates into a product of two *two*-qubit states, $|\Psi\rangle = |\Lambda\rangle_x \otimes |\Omega\rangle_y$. The mapping between the two-qubit state $|\Lambda\rangle_x$ and the parity of the classical pump profile $E_x(x)$ was presented above. A similar mapping holds between $|\Omega\rangle_y$ and $E_y(y)$.

It is important to note that the states $|\Lambda\rangle_x$ and $|\Omega\rangle_y$ do *not* correspond to photon 1 and 2. Each of these states instead spans *both* photons 1 and 2 and relates to their x and y spatial distribution. Both $|\Lambda\rangle_x$ and $|\Omega\rangle_y$ correspond to two-qubit entangled states. In other words, when the pump spatial profile is separable in x and y, the two photons are entangled in x parity *and* in y parity *separately*. We designate this state as doubly entangled. Such a state corresponds to the hyperentangled states produced when different physical DOFs are under consideration and each DOF encodes an entangled logical state. The distinction here is that *both* two-qubit states are encoded in the spatial DOF.

For example, if $E_x(x) = \varphi(x)$ and $E_y(y) = \varphi(y)$, then $|\Lambda\rangle_x = |\Phi^+\rangle_x$ and $|\Omega\rangle_y = |\Phi^+\rangle_y$; i.e., both photons are correlated in the x and y parity, and the 2P-2D state is

$$\begin{aligned}|\Psi\rangle &= |\Phi^+\rangle_x \otimes |\Phi^+\rangle_y = |\Phi^+,\Phi^+\rangle \\ &= \frac{1}{\sqrt{2}}\{|00\rangle + |11\rangle\}_x \otimes \frac{1}{\sqrt{2}}\{|00\rangle + |11\rangle\}_y \\ &= \frac{1}{2}\{|0000\rangle + |0011\rangle + |1100\rangle + |1111\rangle\}. \quad (27)\end{aligned}$$

We identify the logical basis states according to the rule $|0000\rangle = |0\rangle_x^{(1)} \otimes |0\rangle_{x'}^{(2)} \otimes |0\rangle_y^{(1)} \otimes |0\rangle_{y'}^{(2)}$. The superscripts refer to photon 1 and photon 2 of the pair, and the subscripts refer to the x and y coordinates of each photon. We have thus associated the 2P-2D state function $\varphi(x)\varphi(y)\delta(x-x')\delta(y-y')$ with the four-qubit state $|\Phi^+,\Phi^+\rangle$.

By varying the parity of the pump in x and y, we may prepare other Bell-state products. For example, if the separable pump has *even* x parity and *odd* y parity, i.e., $E_x(x) = \varphi(x)$ and $E_y(y) = \varphi(y)u_1(y)$, then the resulting 2P-2D parity state is $|\Phi^+\rangle_x \otimes |\Psi^+\rangle_y = |\Phi^+,\Psi^+\rangle$. We have thus associated the state function $\varphi(x)\varphi(y)u_1(y)\delta(x-x')\delta(y-y')$ with the four-qubit state $|\Phi^+,\Psi^+\rangle$. Similarly, the state $|\Psi^+,\Phi^+\rangle$ ($|\Psi^+,\Psi^+\rangle$) is prepared with a separable pump having odd (odd) x parity and even (odd) y parity (see Table II).

Using the same sequence of separable pump spatial distributions in x and y (even-even, even-odd, odd-even, and odd-odd), all possible products of the four Bell states in x and y parity may be prepared by manipulating the parity of *one* of the photons in the pair. For example, placing $\hat{Z}_x$ in the path of one of the photons, we prepare $|\Phi^-,\Phi^+\rangle$, $|\Phi^-,\Psi^+\rangle$, $|\Psi^-,\Phi^+\rangle$, and $|\Psi^-,\Psi^+\rangle$. Placing instead $\hat{Z}_y$ in the path of that photon, we prepare $|\Phi^+,\Phi^-\rangle$, $|\Phi^+,\Psi^-\rangle$, $|\Psi^+,\Phi^-\rangle$, and $|\Psi^+,\Psi^-\rangle$. Finally, placing both $\hat{Z}_x$ and $\hat{Z}_y$ in the path of that photon, we prepare $|\Phi^-,\Phi^-\rangle$, $|\Phi^-,\Psi^-\rangle$, $|\Psi^-,\Phi^-\rangle$, and $|\Psi^-,\Psi^-\rangle$; see Table II for details.

A new situation arises when the pump is *not* separable in x and y, i.e., when the pump x and y parity are coupled. In this case, it can be shown that the x- and y-parity logical qubit pairs in turn are no longer separable, and we say that the four-qubit state is "cross-entangled": the two DOFs are entangled with each other in the joint Hilbert space.

A *general* four-qubit state takes the form

$$|\Psi\rangle = \sum_{j_n=0,1}^{n=1:4} \alpha_{j_1 j_2 j_3 j_4} |j_1, j_2, j_3, j_4\rangle, \quad (28)$$

represented in the logical (computational) basis. This state inhabits a *16-dimensional Hilbert space* and requires 30 real parameters, within an overall phase and normalization, for the full specification of the complex coefficients $\{\alpha_{j_1 j_2 j_3 j_4}\}$. The 16 products of x- and y-parity Bell states in Table II form an alternative basis for this four-qubit space. In this basis, a general four-qubit state is

$$|\Psi\rangle = \sum_{j=1}^{16} \alpha_j |\Psi_j\rangle, \quad (29)$$

where $|\Psi_j\rangle$ are the Bell-state products. In the spatial representation, the state function of this 2P-2D state is

$$\begin{aligned}\psi(x,y) = &[\{\alpha_1 u_{00}(x,y) + \alpha_2 u_{01}(x,y) + \alpha_3 u_{10}(x,y) + \alpha_4 u_{11}(x,y)\}\delta(x-x')\delta(y-y') \\ &+ \{\alpha_5 u_{00}(x,y) + \alpha_6 u_{01}(x,y) + \alpha_7 u_{10}(x,y) + \alpha_8 u_{11}(x,y)\}\delta(x-x')\delta(y+y') \\ &+ \{\alpha_9 u_{00}(x,y) + \alpha_{10} u_{01}(x,y) + \alpha_{11} u_{10}(x,y) + \alpha_{12} u_{11}(x,y)\}\delta(x+x')\delta(y-y') \\ &+ \{\alpha_{13} u_{00}(x,y) + \alpha_{14} u_{01}(x,y) + \alpha_{15} u_{10}(x,y) + \alpha_{16} u_{11}(x,y)\}\delta(x+x')\delta(y+y')]. \quad (30)\end{aligned}$$

We have thus established a mapping from this family of 2P-2D parity states and the four-qubit states in Eq. (29), and thereby the four-qubit state in Eq. (28).

In order to generate an arbitrary four-qubit pure state [Eq. (28)], four NLCs are required, as shown in Fig. 7, which extends the two-qubit arrangement in Fig. 3 to four qubits.

TABLE II. Preparing 2P-2D parity states using a separable pump. $u_{00}(x,y)=\varphi(x)\varphi(y)$, $u_{01}(x,y)=u_{00}(x,y)u_1(y)$, $u_{10}(x,y)=u_{00}(x,y)u_1(x)$, and $u_{11}(x,y)=u_{00}(x,y)u_1(x)u_1(y)$. The unitary operators $\hat{U}_x$ and $\hat{U}_y$ are placed in the path of the first photon only. The 16 resulting states are all products of Bell states in x and y parity. The spatial representation of the 2P-2D state is $E_{\rm p}(x,y)\delta(x-x')\delta(y-y')$.

Pump $E_{\rm p}(x,y)$	$\hat{U}_x\otimes\hat{U}_y$	2P-2D parity state	Implementation
$u_{00}(x,y)$	$\hat{\mathbb{I}}_x\otimes\hat{\mathbb{I}}_y$	$(\lvert00\rangle+\lvert11\rangle)\otimes(\lvert00\rangle+\lvert11\rangle)=\lvert\Phi^+,\Phi^+\rangle$	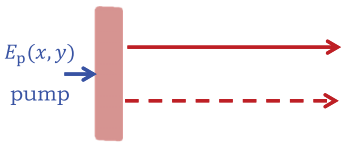
$u_{01}(x,y)$	$\hat{\mathbb{I}}_x\otimes\hat{\mathbb{I}}_y$	$(\lvert00\rangle+\lvert11\rangle)\otimes(\lvert01\rangle+\lvert10\rangle)=\lvert\Phi^+,\Psi^+\rangle$	
$u_{10}(x,y)$	$\hat{\mathbb{I}}_x\otimes\hat{\mathbb{I}}_y$	$(\lvert01\rangle+\lvert10\rangle)\otimes(\lvert00\rangle+\lvert11\rangle)=\lvert\Psi^+,\Phi^+\rangle$	
$u_{11}(x,y)$	$\hat{\mathbb{I}}_x\otimes\hat{\mathbb{I}}_y$	$(\lvert01\rangle+\lvert10\rangle)\otimes(\lvert01\rangle+\lvert10\rangle)=\lvert\Psi^+,\Psi^+\rangle$	
$u_{00}(x,y)$	$\hat{Z}_x\otimes\hat{\mathbb{I}}_y$	$(\lvert00\rangle-\lvert11\rangle)\otimes(\lvert00\rangle+\lvert11\rangle)=\lvert\Phi^-,\Phi^+\rangle$	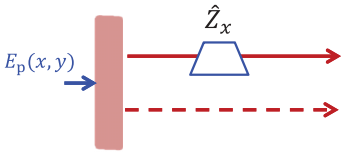
$u_{01}(x,y)$	$\hat{Z}_x\otimes\hat{\mathbb{I}}_y$	$(\lvert00\rangle-\lvert11\rangle)\otimes(\lvert01\rangle+\lvert10\rangle)=\lvert\Phi^-,\Psi^+\rangle$	
$u_{10}(x,y)$	$\hat{Z}_x\otimes\hat{\mathbb{I}}_y$	$(\lvert01\rangle-\lvert10\rangle)\otimes(\lvert00\rangle+\lvert11\rangle)=\lvert\Psi^-,\Phi^+\rangle$	
$u_{11}(x,y)$	$\hat{Z}_x\otimes\hat{\mathbb{I}}_y$	$(\lvert01\rangle-\lvert10\rangle)\otimes(\lvert01\rangle+\lvert10\rangle)=\lvert\Psi^-,\Psi^+\rangle$	
$u_{00}(x,y)$	$\hat{\mathbb{I}}_x\otimes\hat{Z}_y$	$(\lvert00\rangle+\lvert11\rangle)\otimes(\lvert00\rangle-\lvert11\rangle)=\lvert\Phi^+,\Phi^-\rangle$	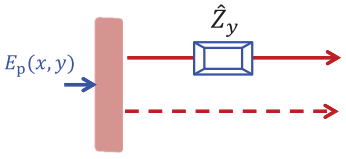
$u_{01}(x,y)$	$\hat{\mathbb{I}}_x\otimes\hat{Z}_y$	$(\lvert00\rangle+\lvert11\rangle)\otimes(\lvert01\rangle-\lvert10\rangle)=\lvert\Phi^+,\Psi^-\rangle$	
$u_{10}(x,y)$	$\hat{\mathbb{I}}_x\otimes\hat{Z}_y$	$(\lvert01\rangle+\lvert10\rangle)\otimes(\lvert00\rangle-\lvert11\rangle)=\lvert\Psi^+,\Phi^-\rangle$	
$u_{11}(x,y)$	$\hat{\mathbb{I}}_x\otimes\hat{Z}_y$	$(\lvert01\rangle+\lvert10\rangle)\otimes(\lvert01\rangle-\lvert10\rangle)=\lvert\Psi^+,\Psi^-\rangle$	
$u_{00}(x,y)$	$\hat{Z}_x\otimes\hat{Z}_y$	$(\lvert00\rangle-\lvert11\rangle)\otimes(\lvert00\rangle-\lvert11\rangle)=\lvert\Phi^-,\Phi^-\rangle$	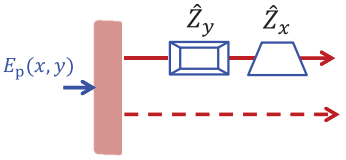
$u_{01}(x,y)$	$\hat{Z}_x\otimes\hat{Z}_y$	$(\lvert00\rangle-\lvert11\rangle)\otimes(\lvert01\rangle-\lvert10\rangle)=\lvert\Phi^-,\Psi^-\rangle$	
$u_{10}(x,y)$	$\hat{Z}_x\otimes\hat{Z}_y$	$(\lvert01\rangle-\lvert10\rangle)\otimes(\lvert00\rangle-\lvert11\rangle)=\lvert\Psi^-,\Phi^-\rangle$	
$u_{11}(x,y)$	$\hat{Z}_x\otimes\hat{Z}_y$	$(\lvert01\rangle-\lvert10\rangle)\otimes(\lvert01\rangle-\lvert10\rangle)=\lvert\Psi^-,\Psi^-\rangle$	

Each NLC has a pump with 2D spatial profile $E_j(x,y)$, $j=1,2,3,4$, which requires six real parameters for the complete specification of its 2D parity: the three relative amplitudes and the three relative phases between the four quadrants of the x-y plane (see Fig. 3). The four pump spatial profiles thus provide 24 real parameters of the four-qubit state. The remaining six parameters derive from the three relative complex weights of the four pumps after fixing the amplitude and phase of one of them, which in turn determines the relative complex weights of the states produced by the four NLCs. Thus, by sculpting the amplitude and phase of the classical optical pump profile, we can encode a four-qubit parity state. Most four-qubit states require less complex optical arrangements for their preparation, compared to the arrangement in Fig. 7 that produces an *arbitrary* four-qubit state with no prior knowledge of the particular state required.

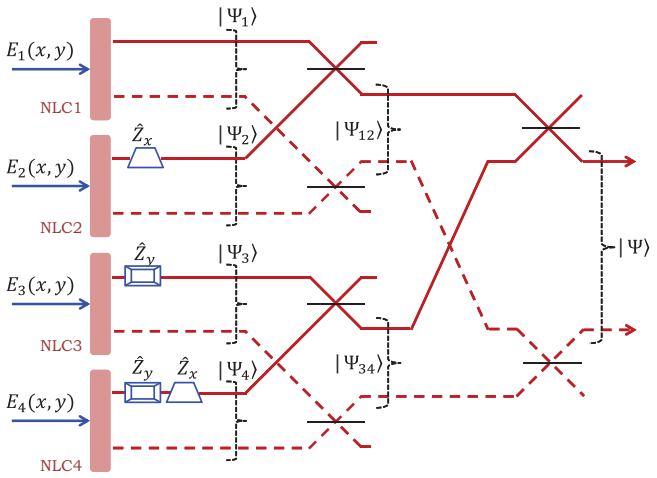

FIG. 7. (Color online) Schematic of a configuration for generating an arbitrary four-qubit state with 30 independent real parameters encoded in the spatial distributions of the classical pumps $E_j(x,y)$, $j=1,2,3,4$ and their relative complex amplitudes. The black horizontal line segments each represent a symmetric nonpolarizing beam splitter.

The question of classification of N-qubit states has attracted considerable attention. There is only one class of two-qubit entangled states and two *distinct* classes of three-qubit-state entanglement: GHZ states, $|{\rm GHZ}_3\rangle=\frac{1}{\sqrt{2}}\{|000\rangle+|111\rangle\}$, and W states, $|W_3\rangle=\frac{1}{\sqrt{3}}\{|001\rangle+|010\rangle+|100\rangle\}$ [75]. The $N=4$ case (four-qubit states) is considerably more complex and some controversy over the proper classification of distinct entanglement classes remains. Two early studies indicated that nine [76] or eight [77] distinct classes of entangled four-qubit states exist. A recent study [78] utilizing tools from string-theory treatment of black holes has identified nine classes of four-qubit entangled states modulo qubit permutations. Using the above-described approach for generating an arbitrary four-qubit 2P-2D parity state, all these families may be generated and studied. We describe the preparation of two particular classes of four-qubit states: GHZ and W states.

B. Four-qubit GHZ states

Although GHZ states are fundamental tools both in tests of the foundations of quantum mechanics and in applications

of quantum information processing, preparation of photonic GHZ states has heretofore proven challenging. The first experimental demonstration of a three-photon GHZ state made use of a four-photon state with one photon heralding the preparation of the GHZ state. No demonstration of a *two-photon GHZ photonic state* has been forthcoming.

Since the four-NLC configuration in Fig. 7 produces an arbitrary four-qubit state, appropriate settings of the experimental parameters will yield the four-qubit GHZ state,

$$|\mathrm{GHZ}_4\rangle = \frac{1}{\sqrt{2}}\{|0000\rangle + |1111\rangle\}. \tag{31}$$

This state may be prepared using the simpler arrangement in Fig. 8(a) that requires two NLCs having the same pump (with equal amplitude and no relative phase) that is separable and has even parity in x and y, $E_1(x,y) = E_2(x,y) = \varphi(x)\varphi(y) = u_{00}(x,y)$. Both NLCs produce the 2P-2D parity state $|\Phi^+,\Phi^+\rangle$. One photon from NLC2 passes spatial flips in x and y, $\hat{Z}_x$ and $\hat{Z}_y$, resulting in the state $(\hat{Z}_x^{(1)} \otimes \mathbb{I}_x^{(2)}) \otimes (\hat{Z}_y^{(1)} \otimes \mathbb{I}_y^{(2)})|\Phi^+,\Phi^+\rangle = |\Phi^-,\Phi^-\rangle$, where the superscripts refer to the two photons produced by NLC2. Superposing the probability amplitudes from the two NLCs results in the 2P-2D state

$$|\Psi\rangle = \frac{1}{\sqrt{2}}\{|\Phi^+,\Phi^+\rangle + |\Phi^-,\Phi^-\rangle\} = |\mathrm{GHZ}_4\rangle. \tag{32}$$

The arrangement may be further simplified to make use of a single NLC, as shown in Fig. 8(b). In this case, photon 1 is split into two paths, one of which contains operators $\hat{Z}_x$ and $\hat{Z}_y$, before being combined to result in $|\mathrm{GHZ}_4\rangle$.

The spatial distribution of the two entangled photons is given by the 2P state function,

$$\psi(x,y;x',y') = u_{00}(x,y) \times \{\delta(x-x')\delta(y-y') + \delta(x+x')\delta(y+y')\}; \tag{33}$$

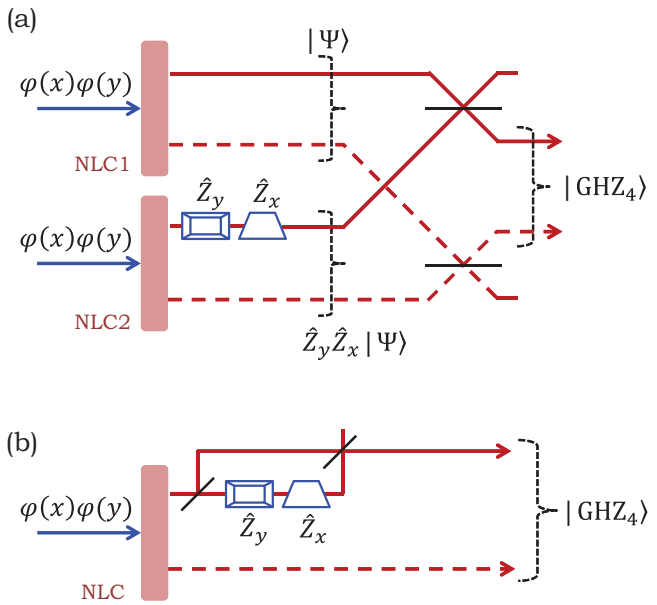

FIG. 8. (Color online) Schematic arrangements for generating the four-qubit 2P-2D GHZ state, $|\mathrm{GHZ}_4\rangle = \frac{1}{\sqrt{2}}\{|0000\rangle + |1111\rangle\}$, using (a) two NLCs or (b) a single NLC.

i.e., the pair is in an equal superposition of being detected at correlated positions or at anti-correlated positions in the planes (x,y) and (x',y'). While both spatially correlated and anticorrelated two-photon states have been previously studied [79,80], the *superposition* of these two states has not, and thus the recognition that such a superposition constitutes a four-qubit GHZ parity state was not hitherto made.

C. Four-qubit *W* states

Another important entangled four-qubit state is the so-called W state. Its importance in QIP derives from the robustness of its entanglement under losses. The four-qubit W state is

$$|W_4\rangle = \tfrac{1}{2}\{|0001\rangle + |0010\rangle + |0100\rangle + |1000\rangle\}. \tag{34}$$

This state may be prepared using the arrangement shown in Fig. 9(a). NLC1 has a pump distribution $\varphi(x)\varphi(y)u_1(y)$, which is even in x and odd in y and produces the state $|\Phi^+,\Psi^+\rangle$. The arrangement in Fig. 9(a) then produces the superposition $|\Psi_1\rangle = \frac{1}{\sqrt{2}}\{|\Phi^+,\Psi^+\rangle + |\Phi^-,\Psi^+\rangle\}$. NLC2 has a pump distribution $\varphi(x)\varphi(y)u_1(x)$, which is odd in x and even in y and produces the state $|\Psi^+,\Phi^+\rangle$. The arrangement in Fig. 9(a) then produces the superposition $|\Psi_2\rangle = \frac{1}{\sqrt{2}}\{|\Psi^+,\Phi^+\rangle + |\Psi^+,\Phi^-\rangle\}$. By superposing $|\Psi_1\rangle$ and $|\Psi_2\rangle$ we obtain

$$|\mathrm{W}_4\rangle = \frac{1}{\sqrt{2}}\{|\Psi_1\rangle + |\Psi_2\rangle\} = \frac{1}{2}\{|\Phi^+,\Psi^+\rangle + |\Phi^-,\Psi^+\rangle + |\Psi^+,\Phi^+\rangle + |\Psi^+,\Phi^-\rangle\}. \tag{35}$$

In the spatial representation, the state function for the 2P-2D W state is

$$\psi(x,y;x',y') = u_{01}(x,y)\delta(y-y')\{\delta(x-x') + \delta(x+x')\} + u_{10}(x,y)\delta(x-x')\{\delta(y-y') + \delta(y+y')\}; \tag{36}$$

$u_{01}(x,y) = \varphi(x)\varphi(y)u_1(y)$ and $u_{10}(x,y) = \varphi(x)\varphi(y)u_1(x)$.

In contrast to the one-photon realization of $|W_4\rangle$ in Ref. [81], where the qubits are encoded in multiple paths of the photon, our realization here encodes the qubits in the spatial profile of the field (specifically, in the spatial distribution of the phase).

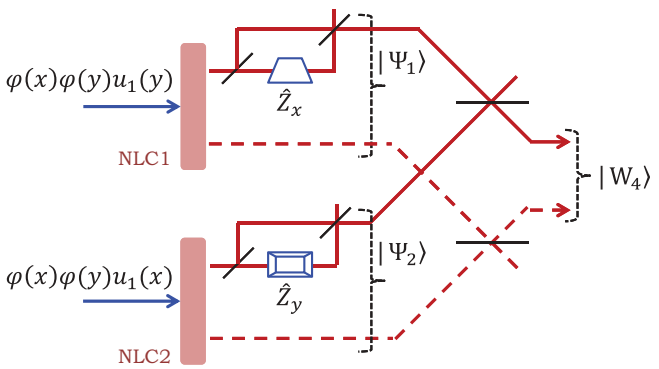

FIG. 9. (Color online) Schematic arrangement for generating the four-qubit 2P-2D W state, $|W_4\rangle = \frac{1}{2}\{|0001\rangle + |0010\rangle + |0100\rangle + |1000\rangle\}$ using two NLCs.

VI. DISCUSSION AND CONCLUSION

We have presented an approach for encoding logical qubits in the spatial parity of one-photon and two-photon states. One qubit is encoded per transverse spatial dimension of the photon. Two qubits are thus encoded in the x and y parity, manipulated separately or jointly using simple linear optical devices, and projected using a modified MZI. Using entangled-photon pairs produced by SPDC, we have theoretically demonstrated that sculpting the classical optical pump together with simple manipulations of the SPDC photons enables the encoding of four entangled spatial parity qubits, two in each photon. We have also described the preparation of an *arbitrary* four-qubit state, one that inhabits a 16-dimensional Hilbert space and requires 30 independent real parameters for its complete specification. The generation of four-qubit GHZ and W states was described in detail.

A further increase in the size of the Hilbert space may be achieved in two different ways. First, a high-intensity ultrafast pump may be used to produce higher-photon-number states and thereby encode a larger number of qubits than studied in this paper. For example, a four-photon state enables the encoding of eight spatial parity qubits. Second, the information-carrying capacity of each photon may be increased by including other DOFs. We have focused solely here on the spatial DOF and overlooked other DOFs, such as polarization and the temporal-spectral DOF. Including polarization alongside 2D parity, for example, enables us to encode three qubits per photon. We will investigate the coupling between polarization and spatial parity elsewhere.

APPENDIX: QUANTUM STATE PRODUCED BY SPDC

The quantum state representing the two-photon field produced by SPDC from an NLC of thickness ℓ is $|\Psi\rangle = \iint d\mathbf{q}_\mathrm{s} d\mathbf{q}_\mathrm{i} \widetilde{\psi}(\mathbf{q}_\mathrm{s},\mathbf{q}_\mathrm{i}) |1_{\mathbf{q}_\mathrm{s}},1_{\mathbf{q}_\mathrm{i}}\rangle$ [14]. Here

$$\widetilde{\psi}(\mathbf{q}_\mathrm{s},\mathbf{q}_\mathrm{i}) = \widetilde{E}_p\left(q_\mathrm{s}^x + q_\mathrm{i}^x, q_\mathrm{s}^y + q_\mathrm{i}^y\right) \widetilde{\chi}(\mathbf{q}_\mathrm{s},\mathbf{q}_\mathrm{i}), \tag{A1}$$

where $\mathbf{q}_\mathrm{t} = (q_\mathrm{t}^x, q_\mathrm{t}^y)$, and $k_\mathrm{t} = 2\pi/\lambda_\mathrm{t}$, t = p,s,i, are the transverse momentum vectors and total momenta of the pump, signal, and idler photons, respectively, and λ_t is the wavelength inside the NLC. The state function $\widetilde{\psi}(\mathbf{q}_\mathrm{s},\mathbf{q}_\mathrm{i})$ is the 4D Fourier transform of $\psi(\mathbf{r},\mathbf{r}')$, where $\mathbf{r} = (x,y)$ and $\mathbf{r}' = (x',y')$ are the 2D vector positions of the signal and idler photons,

$$\psi(\mathbf{r},\mathbf{r}') = \iint d\mathbf{q}_\mathrm{s} d\mathbf{q}_\mathrm{i}\, e^{i\{\mathbf{q}_\mathrm{s}\cdot\mathbf{r} + \mathbf{q}_\mathrm{s}\cdot\mathbf{r}'\}} \widetilde{\psi}(\mathbf{q}_\mathrm{s},\mathbf{q}_\mathrm{i}). \tag{A2}$$

Here $\psi(\mathbf{r},\mathbf{r}')$ represents the correlation in positions of the signal and idler photons, while $\widetilde{\psi}(\mathbf{q}_\mathrm{s},\mathbf{q}_\mathrm{i})$ represents the correlation in their transverse momenta. $\widetilde{E}_\mathrm{p}(q_\mathrm{p}^x, q_\mathrm{p}^y)$ is the 2D Fourier transform of the pump spatial profile $E_\mathrm{p}(x,y)$ at the NLC. Finally, the phase-matching function $\widetilde{\chi}$ depends on the axial wave-number mismatch $\Delta k_z = k_\mathrm{p}^z - k_\mathrm{s}^z - k_\mathrm{i}^z$: $\widetilde{\chi}(\mathbf{q}_\mathrm{s},\mathbf{q}_\mathrm{i}) \propto \exp(i\ell\Delta k_z/2)\,\mathrm{sinc}(\ell\Delta k_z/2\pi)$; here

$$k_\mathrm{p}^z = \sqrt{k_\mathrm{p}^2 - \left(q_\mathrm{s}^x + q_\mathrm{i}^x\right)^2 - \left(q_\mathrm{s}^y + q_\mathrm{i}^y\right)^2},$$
$$k_\mathrm{j}^z = \sqrt{k_\mathrm{j}^2 - \left(q_\mathrm{j}^x\right)^2 - \left(q_\mathrm{j}^y\right)^2}, \quad \mathrm{j} = \mathrm{s,i}.$$

For type-I collinear degenerate phase-matched SPDC, the paraxial approximation leads to $\Delta k_z \approx [(q_\mathrm{s}^x - q_\mathrm{i}^x)^2 + (q_\mathrm{s}^y - q_\mathrm{i}^y)^2]/2k_\mathrm{p}$. We further assume that narrow spectral filters are placed in the path of the signal and idler photons. These simplifications have been found to provide an adequate description of a wide range of quantum-imaging experiments that utilize photon pairs generated by SPDC.

The phase-matching function $\widetilde{\chi}(\mathbf{q}_s,\mathbf{q}_i)$ may be separated, within a very good approximation (Appendix I in Ref. [23]), to yield

$$\begin{aligned}\widetilde{\chi}(\mathbf{q}_s,\mathbf{q}_i) &= \widetilde{\chi}\left(q_s^x - q_i^x, q_s^y - q_i^y\right) \\ &\approx \widetilde{\chi}_1\left(q_s^x - q_i^x\right)\widetilde{\chi}_1\left(q_s^y - q_i^y\right),\end{aligned} \tag{A3}$$

where $\widetilde{\chi}_1(q) = \exp(i\pi\ell q^2/2\lambda_p)\,\mathrm{sinc}(\ell q^2/2\lambda_p)$. This separability is independent of the pump spatial profile and is a consequence solely of phase matching in the NLC. If the pump spatial profile is *separable* in x and y, $E_\mathrm{p}(x,y) = E_x(x)E_y(y)$, then its 2D Fourier transform $\widetilde{E}_\mathrm{p}(q_\mathrm{p}^x, q_\mathrm{p}^y)$ is separable in q_p^x and q_p^y, so that $\widetilde{E}_\mathrm{p}(q_\mathrm{p}^x, q_\mathrm{p}^y) = \widetilde{E}_x(q_\mathrm{p}^x)\widetilde{E}_y(q_\mathrm{p}^y)$, and the state function in turn is separable in x and y:

$$\begin{aligned}\psi(\mathbf{r},\mathbf{r}') &= \psi_x(x,x')\psi_y(y,y') \\ &= E_x\left(\frac{x+x'}{2}\right)\chi_1\left(\frac{x-x'}{2}\right) E_y\left(\frac{y+y'}{2}\right)\chi_1\left(\frac{y-y'}{2}\right);\end{aligned} \tag{A4}$$

where $\chi_1(x)$ is the FT of $\widetilde{\chi}_1(q)$.

If the experimental arrangement does not couple the x and y coordinates and the detectors integrate over y, then we may trace over the y dependence and focus on the 2P-1D state:

$$\begin{aligned}|\Psi\rangle &= \iint dq_s^x\, dq_i^x\, \widetilde{E}_x\left(q_s^x + q_i^x\right)\widetilde{\chi}_1\left(q_s^x - q_i^x\right)\left|1_{q_s^x}, 1_{q_i^x}\right\rangle \\ &= \iint dx\, dx'\, E_x\left(\frac{x+x'}{2}\right)\chi_1\left(\frac{x-x'}{2}\right)|1_x, 1_{x'}\rangle.\end{aligned} \tag{A5}$$

The width of the function χ_1 is on the order of $\sqrt{\ell\lambda_p/8}$ which is typically $\ll W$, where W is the spatial width of $E_x(x)$. The idealized 2P-1D state in Eq. (6) is arrived at by taking $\ell \to 0$, so that $\psi(x,x') \to E_x(x)\delta(x-x')$.

If we retain the y dependence and the pump profile is not separable in x and y, then the state function is

$$\begin{aligned}\psi(\mathbf{r},\mathbf{r}') &= \psi(x,x';y,y') \\ &= E\left(\frac{x+x'}{2}, \frac{y+y'}{2}\right)\chi_1\left(\frac{x-x'}{2}\right)\chi_1\left(\frac{y-y'}{2}\right).\end{aligned} \tag{A6}$$

The separability of the state function thus depends on the pump alone and not the phase matching. The idealized 2P-2D state function in Eq. (25) is arrived at by taking $\ell \to 0$, whereupon $\psi(x,x';y,y') \to E(x,y)\delta(x-x')\delta(y-y')$.

[1] D. Bouwmeester, J.-W. Pan, K. Mattle, M. Eibl, H. Weinfurter, and A. Zeilinger, Nature (London) **390**, 575 (1997).

[2] D. Boschi, S. Branca, F. De Martini, L. Hardy, and S. Popescu, Phys. Rev. Lett. **80**, 1121 (1998).

[3] T. Jennewein, C. Simon, G. Weihs, H. Weinfurter, and A. Zeilinger, Phys. Rev. Lett. **84**, 4729 (2000).

[4] D. S. Naik, C. G. Peterson, A. G. White, A. J. Berglund, and P. G. Kwiat, Phys. Rev. Lett. **84**, 4733 (2000).

[5] W. Tittel, J. Brendel, H. Zbinden, and N. Gisin, Phys. Rev. Lett. **84**, 4737 (2000).

[6] P. Walther, K. J. Resch, T. Rudolph, E. Schenck, H. Weinfurter, V. Vedral, M. Aspelmeyer, and A. Zeilinger, Nature (London) **434**, 169 (2005).

[7] R. Prevedel, P. Walther, F. Tiefenbacher, P. Böhi, R. Kaltenbaek, T. Jennewein, and A. Zeilinger, Nature (London) **445**, 65 (2007).

[8] M. S. Tame, R. Prevedel, M. Paternostro, P. Böhi, M. S. Kim, and A. Zeilinger, Phys. Rev. Lett. **98**, 140501 (2007).

[9] S. E. Harris, M. K. Oshman, and R. L. Byer, Phys. Rev. Lett. **18**, 732 (1967).

[10] D. N. Klyshko, Pis'ma Zh. Eksp. Teor. Fiz. **6**, 490 (1967) [Sov. Phys. JETP Lett. **6**, 23 (1967)].

[11] T. G. Giallorenzi and C. L. Tang, Phys. Rev. **166**, 225 (1968).

[12] D. A. Kleinman, Phys. Rev. **174**, 1027 (1968).

[13] C. K. Hong and L. Mandel, Phys. Rev. A **31**, 2409 (1985).

[14] B. E. A. Saleh, A. F. Abouraddy, A. V. Sergienko, and M. C. Teich, Phys. Rev. A **62**, 043816 (2000).

[15] T. Durt, D. Kaszlikowski, J.-L. Chen, and L. C. Kwek, Phys. Rev. A **69**, 032313 (2004).

[16] T. Vértesi, S. Pironio, and N. Brunner, Phys. Rev. Lett. **104**, 060401 (2010).

[17] W.-B. Gao, C.-Y. Lu, X.-C. Yao, P. Xu, O. Gühne, A. Goebel, Y.-A. Chen, C.-Z. Peng, Z.-B. Chen, and J.-W. Pan, Nat. Phys. **6**, 331 (2010).

[18] C.-Y. Lu, X.-Q. Zhou, O. Gühne, W.-B. Gao, J. Zhang, Z.-S. Yuan, A. Goebel, T. Yang, and J.-W. Pan, Nat. Phys. **3**, 91 (2007).

[19] Y.-F. Huang, B.-H. Liu, L. Peng, Y.-H. Li, L. Li, C.-F. Li, and G.-C. Guo, Nature Commun. **2**, 546 (2011).

[20] C. K. Law and J. H. Eberly, Phys. Rev. Lett. **92**, 127903 (2004).

[21] S. L. Braunstein and P. van Loock, Rev. Mod. Phys. **77**, 513 (2005).

[22] V. Giovannetti, S. Lloyd, and L. Maccone, Nature Photon. **5**, 222 (2011).

[23] A. F. Abouraddy, T. Yarnall, B. E. A. Saleh, and M. C. Teich, Phys. Rev. A **75**, 052114 (2007).

[24] T. Yarnall, A. F. Abouraddy, B. E. A. Saleh, and M. C. Teich, Phys. Rev. Lett. **99**, 170408 (2007).

[25] T. Yarnall, A. F. Abouraddy, B. E. A. Saleh, and M. C. Teich, Phys. Rev. Lett. **99**, 250502 (2007).

[26] J. G. Rarity and P. R. Tapster, Phys. Rev. Lett. **64**, 2495 (1990).

[27] M. Fiorentino and F. N. C. Wong, Phys. Rev. Lett. **93**, 070502 (2004).

[28] M. Fiorentino, T. Kim, and F. N. C. Wong, Phys. Rev. A **72**, 012318 (2005).

[29] L. Neves, G. Lima, J. G. Aguirre Gómez, C. H. Monken, C. Saavedra, and S. Pádua, Phys. Rev. Lett. **94**, 100501 (2005).

[30] M. N. O'Sullivan-Hale, I. A. Khan, R. W. Boyd, and J. C. Howell, Phys. Rev. Lett. **94**, 220501 (2005).

[31] S. P. Walborn, D. S. Lemelle, M. P. Almeida, and P. H. Souto Ribeiro, Phys. Rev. Lett. **96**, 090501 (2006).

[32] A. Mair, A. Vaziri, G. Weihs, and A. Zeilinger, Nature (London) **412**, 313 (2001).

[33] M. Reck, A. Zeilinger, H. J. Bernstein, and P. Bertani, Phys. Rev. Lett. **73**, 58 (1994).

[34] M. Żukowski, A. Zeilinger, and M. A. Horne, Phys. Rev. A **55**, 2564 (1997).

[35] G. Weihs, M. Reck, H. Weinfurter, and A. Zeilinger, Phys. Rev. A **54**, 893 (1996).

[36] A. Rossi, G. Vallone, A. Chiuri, F. De Martini, and P. Mataloni, Phys. Rev. Lett. **102**, 153902 (2009).

[37] A. Peruzzo, A. Laing, A. Politi, T. Rudolph, and J. L. O'Brien, Nature Commun. **2**, 224 (2011).

[38] J. W. Goodman, *Introduction to Fourier Optics*, 3rd ed. (Roberts & Company Publishers, Greenwood Village, CO, 2005).

[39] A. W. Lohmann, J. Opt. Soc. Am. A **10**, 2181 (1993).

[40] H. M. Ozaktas, Z. Zalevsky, and M. A. Kutay, *The Fractional Fourier Transform* (Wiley, Chichester, 2001).

[41] S. P. Walborn, D. S. Lemelle, D. S. Tasca, and P. H. Souto Ribeiro, Phys. Rev. A **77**, 062323 (2008).

[42] L. Allen, M. W. Beijersbergen, R. J. C. Spreeuw, and J. P. Woerdman, Phys. Rev. A **45**, 8185 (1992).

[43] L. Allen, S. M. Barnett, and M. J. Padgett, *Optical Angular Momentum* (Institute of Physics Publishing, Bristol, 2003).

[44] H. Di Lorenzo Pires, H. C. B. Florijn, and M. P. van Exter, Phys. Rev. Lett. **104**, 020505 (2010).

[45] A. C. Dada, J. Leach, G. S. Buller, M. J. Padgett, and E. Andersson, Nat. Phys. **7**, 677 (2011).

[46] A. Vaziri, G. Weihs, and A. Zeilinger, Phys. Rev. Lett. **89**, 240401 (2002).

[47] A. Vaziri, J.-W. Pan, T. Jennewein, G. Weihs, and A. Zeilinger, Phys. Rev. Lett. **91**, 227902 (2003).

[48] P. G. Kwiat, J. Mod. Opt. **44**, 2173 (1997).

[49] M. Atatüre, G. Di Giuseppe, M. D. Shaw, A. V. Sergienko, B. E. A. Saleh, and M. C. Teich, Phys. Rev. A **65**, 023808 (2002).

[50] G. Di Giuseppe, M. Atatüre, M. D. Shaw, A. V. Sergienko, B. E. A. Saleh, and M. C. Teich, Phys. Rev. A **66**, 013801 (2002).

[51] M. Atatüre, G. Di Giuseppe, M. D. Shaw, A. V. Sergienko, B. E. A. Saleh, and M. C. Teich, Phys. Rev. A **66**, 023822 (2002).

[52] J. T. Barreiro, N. K. Langford, N. A. Peters, and P. G. Kwiat, Phys. Rev. Lett. **95**, 260501 (2005).

[53] Z.-B. Chen, J.-W. Pan, Y.-D. Zhang, Č. Brukner, and A. Zeilinger, Phys. Rev. Lett. **90**, 160408 (2003).

[54] T. Yang, Q. Zhang, J. Zhang, J. Yin, Z. Zhao, M. Żukowski, Z.-B. Chen, and J.-W. Pan, Phys. Rev. Lett. **95**, 240406 (2005).

[55] M. Barbieri, C. Cinelli, P. Mataloni, and F. De Martini, Phys. Rev. A **72**, 052110 (2005).

[56] G. Vallone, R. Ceccarelli, F. De Martini, and P. Mataloni, Phys. Rev. A **79**, 030301(R) (2009).

[57] R. Ceccarelli, G. Vallone, F. De Martini, P. Mataloni, and A. Cabello, Phys. Rev. Lett. **103**, 160401 (2009).

[58] G. Vallone, E. Pomarico, F. De Martini, and P. Mataloni, Phys. Rev. Lett. **100**, 160502 (2008).

[59] G. Vallone, G. Donati, R. Ceccarelli, and P. Mataloni, Phys. Rev. A **81**, 052301 (2010).

[60] Z.-B. Chen, J.-W. Pan, G. Hou, and Y.-D. Zhang, Phys. Rev. Lett. **88**, 040406 (2002).

[61] Č. Brukner, M. S. Kim, J.-W. Pan, and A. Zeilinger, Phys. Rev. A **68**, 062105 (2003).
[62] M. Revzen, P. A. Mello, A. Mann, and L. M. Johansen, Phys. Rev. A **71**, 022103 (2005).
[63] J. S. Bell, Physics (Long Island City, NY) **1**, 195 (1964).
[64] A. Einstein, B. Podolsky, and N. Rosen, Phys. Rev. **47**, 777 (1935).
[65] J. Leach, B. Jack, J. Romero, M. Ritsch-Marte, R. W. Boyd, A. K. Jha, S. M. Barnett, S. Franke-Arnold, and M. J. Padgett, Opt. Express **17**, 8287 (2009).
[66] J. Leach, B. Jack, J. Romero, A. K. Jha, A. M. Yao, S. Franke-Arnold, D. G. Ireland, R. W. Boyd, S. M. Barnett, and M. J. Padgett, Science **329**, 662 (2010).
[67] F. M. Miatto, A. M. Yao, and S. M. Barnett, Phys. Rev. A **83**, 033816 (2011).
[68] A. F. Abouraddy, T. M. Yarnall, and B. E. A. Saleh, Opt. Lett. **36**, 4683 (2011).
[69] T. Yarnall, A. F. Abouraddy, B. E. A. Saleh, and M. C. Teich, Opt. Express **16**, 7634 (2008).
[70] A. F. Abouraddy, B. E. A. Saleh, A. V. Sergienko, and M. C. Teich, J. Opt. Soc. Am. B **19**, 1174 (2002).
[71] A. F. Abouraddy, B. E. A. Saleh, A. V. Sergienko, and M. C. Teich, Phys. Rev. A **64**, 050101(R) (2001).
[72] S. Hill and W. K. Wootters, Phys. Rev. Lett. **78**, 5022 (1997).
[73] W. K. Wootters, Phys. Rev. Lett. **80**, 2245 (1998).
[74] J. F. Clauser, M. A. Horne, A. Shimony, and R. A. Holt, Phys. Rev. Lett. **23**, 880 (1969).
[75] W. Dür, G. Vidal, and J. I. Cirac, Phys. Rev. A **62**, 062314 (2000).
[76] F. Verstraete, J. Dehaene, B. DeMoor, and H. Verschelde, Phys. Rev. A **65**, 052112 (2002).
[77] L. Lamata, J. León, D. Salgado, and E. Solano, Phys. Rev. A **75**, 022318 (2007).
[78] L. Borsten, D. Dahanayake, M. J. Duff, A. Marrani, and W. Rubens, Phys. Rev. Lett. **105**, 100507 (2010).
[79] B. M. Jost, A. V. Sergienko, A. F. Abouraddy, B. E. A. Saleh, and M. C. Teich, Opt. Express **3**, 81 (1998).
[80] H. Di Lorenzo Pires and M. P. van Exter, Phys. Rev. A **79**, 041801 (2009).
[81] S. B. Papp, K. S. Choi, H. Deng, P. Lougovski, S. J. van Enk, and H. J. Kimble, Science **324**, 764 (2009).